AN ABSTRACT OF THE THESIS OF

Ethan P. Matty for the degree of Master of Science in Mechanical Engineering

presented on June 1, 2021.

Title: Condensation of a Zeotropic Mixture, R-454C, and its Individual Components, R-1234yf and R-32, in Microfin Tubes

Abstract approved: ______________________________

Brian M. Fronk

This work compares the condensation heat transfer and pressure drop for zeotropic refrigerant R-454C and its individual components, R-32 and R-1234yf, in horizontal microfin tubes. One microfin tube has a 4 mm outer diameter, 0.18 mm wall thickness, and a surface area ratio of 1.56. The second tube has a 8 mm outer diameter, 0.25 mm wall thickness and a surface area ratio of 1.62. HFOs and HFC/HFO blends like R-454C have low global warming potential and can be alternatives to HFC refrigerants when retrofitting a system or producing new equipment. However, there is an additional mass transfer resistance present during phase change for a zeotropic mixture, which results in reduced heat transfer performance. Microfin tubes enhance heat transfer through multiple mechanisms: they increase the internal surface area of the tube, the fins drain condensate from the fin tip to the trough region, and they produce secondary flow structures. These

enhancement mechanisms are shown to counteract the degradation in heat transfer performance for R-454C in the 4 mm microfin tube.

Presently, there is limited data of HFO/HFC mixtures in microfin tubes. Thus, experiments are conducted for complete condensation of R-454C, R-1234yf and R-32 for saturation temperatures of 40, 50 and 60 °C and mass fluxes from 50 to $600\,\mathrm{kg\,m^{-2}\,s^{-1}}$. Experimental heat transfer and pressure drop measurements are compared to well-established correlations from the literature. Heat transfer enhancement factors and pressure drop penalty factors are used to determine the optimum operating conditions for the microfin tubes.

Condensation of a Zeotropic Mixture, R-454C, and its Individual Components, R-1234yf and R-32, in Microfin Tubes

by

Ethan P. Matty

A THESIS

submitted to

Oregon State University

in partial fulfillment of
the requirements for the
degree of

Master of Science

Presented June 1, 2021
Commencement June 2022

Master of Science thesis of Ethan P. Matty presented on June 1, 2021.

APPROVED:

Major Professor, representing Mechanical Engineering

Head of the School of Mechanical, Industrial, and Manufacturing Engineering

Dean of the Graduate School

Ethan P. Matty, Author

ACKNOWLEDGEMENTS

I would like to acknowledge Dr. Brian M. Fronk for extending many opportunities to me while I was an undergraduate research assistant, and for being a great mentor through my graduate coursework and research. Your guidance and support during my undergraduate experiences in the lab motivated my decision to pursue a master's degree. Working with you on assessment projects at the Energy Efficiency Center contributed to my professional development and skills that I will take with me to a position in industry.

I am thankful for the financial support that I received from the U.S. Department of Energy through the Industrial Assessment Center program at Oregon State University. I would like to thank Mr. Joseph F. Junker, Director of the Industrial Assessment Center, for supporting me and helping me develop professionally. The skills that I learned as an energy analyst and operations manager will help me be successful in my career.

I would like to thank my colleagues in the TEST Lab for providing support and feedback during my design reviews and presentations. The collaborative lab environment has always been a pleasure to work in.

I would also like to acknowledge Dr. Joshua Gess, Dr. Nordica MacCarty, and Dr. Matthew Johnston for serving on my graduate advisory committee.

Last but certainly not least, I would like to thank my family and friends for their support throughout my undergraduate and graduate coursework and research. This work would not have been possible without them.

TABLE OF CONTENTS

Page

TABLE OF CONTENTS (Continued)

Page

LIST OF FIGURES

LIST OF FIGURES (Continued)

LIST OF FIGURES (Continued)

Figure | Page

LIST OF TABLES

Chapter 1: Introduction

Condensation heat transfer plays a critical role in many engineering processes including power generation, heating and cooling, refrigeration, and chemical processing. Two characteristics of condensation heat transfer make it attractive for engineering applications: (1) high heat transfer coefficients, and (2) isothermal phase change. High heat transfer coefficients associated with phase change processes make it an efficient way to manage large thermal loads in compact applications. Isothermal phase change is a characteristic of pure fluids and azeotropic mixtures. Isothermal phase change is beneficial since it resembles the constant temperature heat rejection process of the Carnot cycle and results in increased thermodynamic efficiency. There are many modes of condensation heat transfer that can be utilized depending on the technical application, but internal convective condensation is a prevalent mode in industry and will be the focus of this work.

Refrigerant regulations have driven the adoption of environmentally friendly hydroolefin (HFO) refrigerants designed to replace refrigerants with high global warming potential (GWP), namely hydrofluorocarbon (HFC) refrigerants. HFO/HFC refrigerant mixtures are attractive replacements because their composition can be adjusted to meet environmental regulations while maintaining desirable thermophysical properties. Mixtures are generally classified based on the temperature glide they exhibit during phase change at constant pressure; phase change occurs isothermally for an azeotropic mixture, and non-isothermally for a zeotropic mixture. There is a degradation in heat transfer performance for zeotropic mixtures due to the additional mass transfer and sensible resistances that are present during condensation. The degradation in heat transfer performance associated with a zeotropic mixture can potentially be counteracted by utilizing a heat transfer enhancement method.

Common heat transfer enhancement methods include integral surface roughness, surface grooves or fins, and insert flow devices such as coil-springs and twisted-tapes. With any modification, the increased heat transfer benefit must be compared to the penalty of increased pressure drop. Internal microfin tubes are widely used in the Heating, Ventilation, Air Conditioning, and Refrigeration (HVAC&R) industry due to considerable heat transfer enhancement with minimal increase in pressure drop (Webb and Kim, 2005). However, with the advent of new refrigerants and refrigerant mixtures, it is necessary to reevaluate the predictive capability of heat transfer and pressure drop correlations, and to assess if heat transfer degradation due to mixture effects can be mitigated using enhanced tubes. Engineers need to have accurate heat transfer and pressure drop correlations to design safe and effective equipment.

Presently, there is limited data for condensation of HFO refrigerants and HFO/HFC zeotropic mixtures in microfin tubes. Thus, in this study, the heat transfer and pressure drop characteristics of R-454C and its individual components are investigated in four microfin tubes over a range of operating conditions. Experimental heat transfer and pressure drop measurements are compared to well-established correlations from the literature. The results from this study will (1) determine which heat transfer and pressure drop correlations perform best for condensation of new refrigerants in microfin tubes, (2) assess if degradation due to mixture effects can be offset by using internally enhanced tubes, and (3) identify the optimum range of operating conditions for condensers that utilize microfin tubes.

1.1 Motivation

Refrigerant regulations, such as the Kigali amendment to the Montreal Protocol and the European Union fluorinated greenhouse gas (F-gas) regulations, have driven the adoption of environmentally friendly refrigerant mixtures designed to replace refrigerants with high GWP. The Kigali amendment was ratified in 2016 with support from over 170 countries. The amendment specifies the timetable for reducing the production and consumption of HFC refrigerants. HFC refrigerants were originally brought to market because they do not deplete the ozone layer. Compared to chlorofluorocarbon (CFC) refrigerants, this was a significant improvement. However, HFCs are potent greenhouse gases. The GWP of CO_2 is used as a baseline for assessing the GWP of other gases, such as refrigerants. For example, CO_2 has a GWP of 1 and the GWP of HFC refrigerants varies from 53 to 14,800. The Kigali amendment outlines two phase down paths; one path is for developing countries, and the second path is for developed countries. The phase down timetables are based on HFC consumption over a 3-year baseline period from 2011 to 2013. Ultimately, the phase down timetables aim to reduce the consumption and production of HFC refrigerants by 85% by the year 2036 (*Amendment to the Montreal Protocol on Substances That Deplete the Ozone Layer* 2016).

In 2006, the European Union regulated the impact of F-gases by focusing on reducing emissions from system leaks and by enforcing refrigerant recovery for decommissioned equipment. These F-gas regulations were updated in 2014 to restrict the production and use of fluorinated gases, which include HFCs. The phase down timeline aims to reduce F-gas emissions by 78%, compared to 1990 levels, by 2050 (*Regulation (EU) No 517/2014 of the European Parliament and of the Council of 16 April 2014 on fluorinated greenhouse gases and repealing Regulation (EC) No 842/2006* 2014).

New refrigerants with low GWP must be used in the next generation of HVAC&R equipment to reduce the environmental impact of operating heating and cooling equipment and to comply with environmental regulations. Most HVAC&R systems generate the desired heating or cooling effect using a vapor-compression cycle. The components of a vapor-compression system include the evaporator, compressor, condenser, and an expansion device. For a refrigeration cycle, the refrigerant is vaporized in the evaporator as energy is removed from the refrigerated space. The vaporized refrigerant is them compressed to a high pressure and temperature by the compressor. In the condenser, heat is transferred to the ambient and the refrigerant condenses. Finally, the high-pressure refrigerant is expanded to the evaporator pressure and the cycle repeats.

There are many factors to consider when selecting a working fluid for a vapor-compression system including environmental acceptability, chemical stability, material compatibility, cycle performance, and toxicity. The rate of energy removal from the refrigerated space is the refrigeration capacity. The refrigeration capacity and the thermophysical properties of the refrigerant are used to determine the mass flow rate of refrigerant in the system. The size of the evaporator and condenser are determined by the heat transfer and pressure drop characteristics of the working fluid. The pressure drop throughout the system increases the required parasitic pumping power, and therefore, reduces the refrigeration coefficient of performance (COP). In the condenser and evaporator, any pressure drop also reduces the saturation temperature, which can lead to temperature pinch effects. Therefore, it is critical to accurately predict the heat transfer and pressure drop performance of new refrigerants and refrigerant mixtures so new equipment can be effective and efficient.

The focus of this study is zeotropic refrigerant mixture R-454C. R-454C is a zeotropic mixture of R-32 and R-1234yf (21.5/78.5 wt%) with a GWP of 146 that can replace R-404a and R-22 in newly manufactured low and medium temperature commercial and industrial refrigeration systems (*Opteon XL20* 2016). It has a temperature glide of 6 K (i.e., the difference between the dew point and bubble point at a given pressure). Experiments are also conducted with the pure constituent components, R-32 and R-1234yf. R-32 is an HFC with a GWP of 675 and is used in supermarket refrigeration as well as commercial and residential air conditioning and heat pump applications. It is a drop-in replacement for R-410a. R-1234yf is an HFO and is a drop-in replacement for R-134a in automotive air conditioning applications and has a GWP of 4. The lessons learned from this mixture are expected to extrapolate to other similar HFO/HFC mixtures.

1.2 Mixture condensation

Mixture condensation can generally be categorized as azeotropic, near-azeotropic, or zeotropic. These three classes of mixtures can be distinguished as follows: during condensation at constant pressure, a zeotropic mixture exhibits a nonisothermal phase change, a near-azeotropic mixture exhibits a small temperature glide ($\lesssim 5K$), and an azeotrope mixture exhibits no temperature glide. The range of saturation temperature observed during phase change is called the temperature glide, and it is dependent upon the species present and the composition of the mixture. The condensation phenomena for an azeotropic mixture is similar to condensation of a pure fluid because the equilibrium composition of the liquid and vapor phases are the same as vapor quality decreases from one to zero.

A phase diagram for R-32/R-1234yf is shown in Figure 1.1 to illustrate the change in temperature and change in equilibrium composition of the liquid and vapor phases that occur during condensation at 2000 kPa. The dew point line, shown in red, is the temperature plotted as a function of the vapor mole fraction of R-32. The bubble point line, shown in blue, is the temperature plotted as a function of the liquid mole fraction of R-32. Above the dew point line the mixture is a superheated vapor, and below the bubble point line the mixture is a subcooled liquid. On the horizontal axis, mole fractions of zero and one correspond to pure R-1234yf and pure R-32, respectively. As shown, R-32 has a lower saturation temperature at

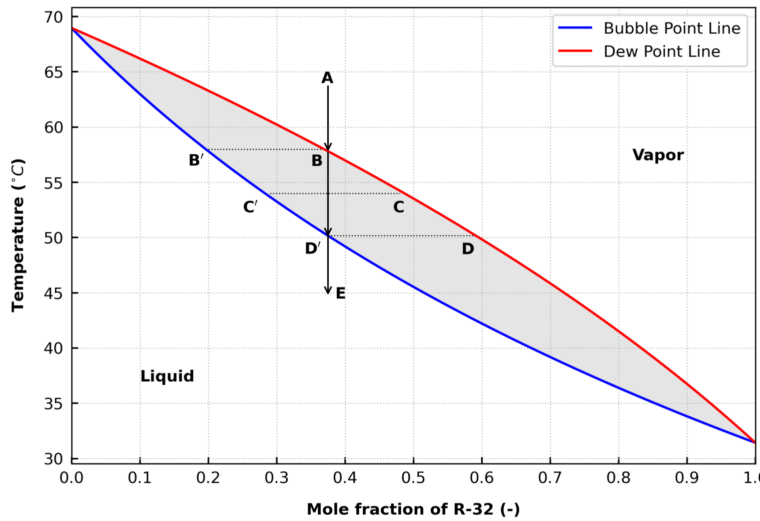

Figure 1.1: A phase equilibrium diagram of R-32/R-1234yf mixtures at 2000 kPa.

this pressure and is the more volatile component in the mixture. The condensation process for R-454C, a mixture of R-32 and R-1234yf (21.5/78.5 wt%), is overlaid on Figure 1.1. Starting at point A, the mixture is a superheated vapor. The mixture is then cooled at constant pressure until the dew point temperature is reached at point B. Here, condensation begins.

At point B, the mole fraction of R-32 in the vapor is equal to the overall mole fraction of R-32 in the mixture. The mole fraction of R-32 in the first drop of liquid formed can be read from the intersection of the tie line and the bubble point line, point B'. At point B', the mole fraction of R-32 is less than the mole fraction of R-1234yf in the liquid phase. Preferential condensation of R-1234yf occurs because it is the less-volatile component in the mixture, as indicated by the higher saturation temperature at 2000 kPa. As condensation proceeds, the mole fraction of R-32 increases in the liquid phase as shown by the progression from B'

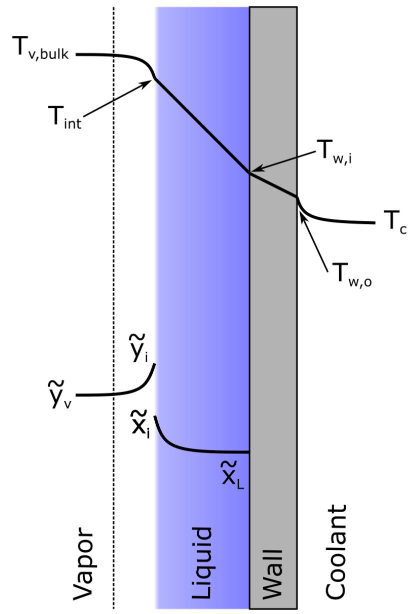

Figure 1.2: Schematic of film condensation of a binary zeotropic mixture.

to D' along the bubble point line, and similarly for the liquid phase from B to D along the dew point line. At D' the mole fraction of R-32 in the liquid phase is equal to the overall mole fraction of R-32 in the mixture. With further cooling, the mixture is a subcooled liquid as indicated at point E.

The assumption of thermodynamic equilibrium is used to generate the phase diagram in Figure 1.1. However, phase change processes are inherently non-equilibrium processes. As condensation proceeds for the mixture, temperature and concentration gradients develop between the vapor bulk and interface, and the liquid bulk and interface. Figure 1.2 shows a schematic of the temperature and concentration gradients that develop during film condensation of a zeotropic mixture.

As mentioned previously, the less-volatile component condenses preferentially when the mixture is cooled to the dew point. This results in an accumulation of the more-volatile component at the interface. From Figure 1.1, if the mole fraction of R-32 increases along the dew point line, the temperature decreases. This results in the depression of the interface temperature, which is ultimately responsible for the degradation in heat transfer associated with zeotropic mixtures. Additionally, the concentration gradient in the vapor phase causes the more-volatile component to diffuse towards the interface and the less-volatile component to diffuse away from the interface. For molecules to reach the interface and condense, they must travel through this diffusion layer and, as a result, mass transfer resistances must be included when modeling zeotropic condensation processes. A concentration gradient also develops in the liquid phase. In summary, the overall condensation rate is directly related to the driving temperature difference between the vapor bulk and the interface, and the interface temperature is directly related to the interfacial concentration. Therefore, heat and mass transfer and strongly coupled for condensation of zeotropic mixtures.

1.3 Heat transfer enhancement

In some applications, it may be desired or required to enhance condensation heat transfer to make heat exchangers more compact and efficient. Several heat transfer enhancement methods have been investigated with the objective of making heat exchangers more compact and efficient. They can generally be categorized as active or passive. Active techniques require external power to produce the enhancement, while passive enhancement techniques do not require external power. Passive techniques enhance heat transfer by utilizing coated surfaces, rough surfaces, insert flow devices such as twisted-tapes or coil springs, surface flutes, grooves, or fins, to name a few. Passive techniques are commonly implemented due to their lower implementation cost and increased reliability (Webb and Kim, 2005). For rough surfaces, extended surfaces, and insert flow devices, enhanced performance is achieved by increasing the surface area, the heat transfer coefficient, or both.

There are four performance improvements that can be utilized by the use of an enhanced surface, with a refrigeration system used as an example, they are:

1. Reduced heat transfer surface area for the evaporator for fixed compressor power

2. Increased evaporator heat duty for fixed compressor lift

3. Reduced compressor power for fixed evaporator heat duty

4. The log-mean temperature difference for the evaporator or condenser can be reduced, resulting in reduced compressor lift (and therefore compressor power).

Utilizing an enhanced surface can provide any one of these performance improvements. For internal convective condensation, finned tubes, rough surfaces, twisted-tape inserts, and wire-coil inserts have all been investigated (Webb and Kim, 2005). Of these methods, the microfin tube has received considerable attention since

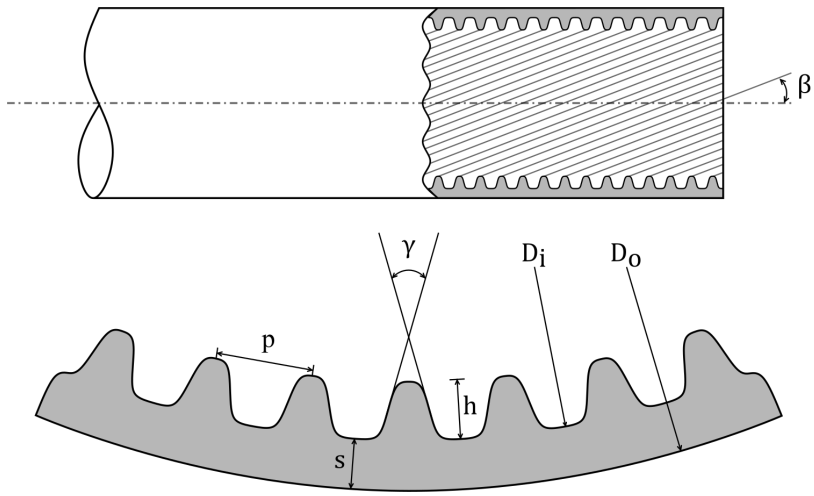

Figure 1.3: Characteristic geometries of a microfin tube.

its invention in 1977 by researchers at Hitachi Cable, Ltd. (Webb and Kim, 2005). This is primarily due to the appreciable heat transfer enhancement with minimal increase in pressure drop. Additionally, microfin tubes are manufactured by cold drawing a smooth tube through a rotating die, which is similar to manufacturing seamless tubes. Alternatively, the fin geometry can be embossed onto a flat sheet of metal, and the strip can be rolled and welded down the seam. The microfin tube is commercially available in a wide range of tube of fin geometries because these manufacturing techniques scale easily to the industrial level. The characteristic geometries of a microfin tube are shown in Figure 1.3.

Considerable work has been done to optimize fin geometries for condensation and boiling applications. Microfin tubes have internal fins that are typically less than a millimeter tall, helix angles from $15 - 40°$, and 36-82 fins depending on the tube diameter. The fins enhance condensation heat transfer by increasing the

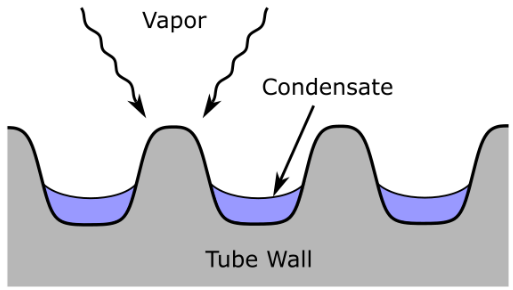

Figure 1.4: A schematic of surface tension driven condensate drainage for microfins.

internal surface area of the tube, producing secondary flow patterns, and draining condensate from the tip of the fin to the trough region, as shown in Figure 1.4. Microfin tubes are geometrically optimized to reduce material use, making them economical and lightweight.

The heat transfer benefits of using microfin tubes can potentially counteract the degradation in heat transfer for zeotropic mixtures. As zeotropic mixtures replace HFC refrigerants, new equipment can be designed with microfin tubes to counteract the degradation in heat transfer associated with zeotropic mixtures. In order to design effective equipment, engineers must have accurate predictive correlations for heat transfer and pressure drop of next generation refrigerants in microfin tubes.

1.4 Thesis Organization

The chapters in this thesis are structured in the following manner:

- Chapter 2 presents a review of previous investigations into refrigerant condensation in smooth and microfin tubes for both pure fluids and refrigerant mixtures. The heat transfer enhancement and pressure drop penalty characteristics for microfin tubes are introduced. Heat transfer and pressure drop modeling efforts are also reviewed. Heat transfer and pressure drop correlations, flow visualization studies, and analytical modeling methods are also explored.

- Chapter 3 provides details about the experimental facility used to conduct this investigation. The data reduction methodology is outlined for calculating quasi-local heat transfer coefficients and condensation frictional pressure drop.

- The condensation heat transfer and pressure drop results are presented in Chapter 4. The measured data is also compared to correlations from the literature.

- Chapter 5 explores the performance improvements that are made available by utilizing a microfin tube compared to a smooth tube in condensers.

- Chapter 6 presents the conclusions from this study, and identifies relevant topics for future investigations.

Chapter 2: Literature Review

Some of the earliest investigations of enhancing in-tube condensation heat transfer were conducted with insert flow devices such as twisted tapes and wire coil inserts (Webb and Kim, 2005). Twisted tapes are made by twisting a thin rectangular strip of metal into a continuous helical form, and wire coil inserts resemble springs. Fin effects are irrelevant because these devices generally have poor thermal contact with the tube's inner surface. The poor thermal contact is a result of the small clearance between the device and the tube wall because the device has to be inserted into the smooth tube.

In the 1960s, advances in manufacturing techniques made it possible to create internally finned tubes, and investigations with these tubes became more prevalent. Royal and Bergles (1978) found that spirally finned tubes enhanced heat transfer coefficients by as much as 150% compared to a smooth tube, while the twisted tape inserts produced a 30% increase in heat transfer coefficients. The increase in frictional pressure drop for the twisted-tapes was greater than the increase in heat transfer coefficients making the finned tubes a better choice for enhanced performance.

Internally finned tubes are now commercially available because manufacturing methods are similar to those for making smooth tubes. An axially finned tube can be made by extruding a smooth tube through a die, and a helically finned tube can be made with a rotating die. The ratio of the fin height and the fin root diameter, e/d_i, distinguishes microfin tubes from finned tubes in general. Microfin tubes have $e/d_i < 0.05$, where e is the fin height and d_i is the fin root diameter (Webb and Kim, 2005). The microfin tube was patented by researchers at Hitachi Cable, Ltd. in 1977, and was designed to enhance heat transfer for two-phase flows and reduce the weight per unit length of tube (Webb and Kim, 2005). The heat transfer enhancement and frictional pressure drop increase in a microfin tube are frequently compared to equivalent operating conditions in smooth tubes. The ratio of the heat transfer coefficient, α, in a microfin tube over a smooth tube is defined as the enhancement factor, Equation 2.1. The penalty factor is defined analogously, but with frictional pressure drop, ΔP_{fr}, as shown in Equation 2.2.

$$EF = \frac{\alpha_{microfin}}{\alpha_{smooth}} \tag{2.1}$$

$$PF = \frac{\Delta P_{fr,microfin}}{\Delta P_{fr,smooth}} \tag{2.2}$$

This review focuses on condensation of single-component and multi-component refrigerants in horizontal internally finned tubes and microfin tubes. This review begins with an overview of condensation of pure refrigerants in smooth tubes, then transitions to condensation in microfin tubes. The mechanisms of heat transfer enhancement in microfin tubes and the effects of varying the fin geometry will also be discussed. Additionally, recent two-phase flow visualization studies in microfin tubes and numerical modeling efforts will be discussed. Then, condensation of zeotropic refrigerant mixtures will be emphasized and current gaps in the literature will be identified.

Throughout this review, the terms finned tube and grooved tube are used interchangeably. The enhancement factor may also be referred to as the enhancement ratio, and the same goes for the penalty factor. The helix angle of a finned tube may also be referred to as the spiral angle. These terms are used interchangeably in the literature and they will all appear in this literature review specified in the original source.

2.1 Pure fluid condensation

Internal convective condensation commonly occurs in tubes in the horizontal orientation. As condensation proceeds along the length of the tube, the local flow pattern changes. The sequence of flow regimes depends on the fluid flow rate, fluid properties, vapor quality, void fraction, tube diameter and orientation of the tube. The local flow regime has a large impact on the heat transfer characteristics and pressure drop. When a flow of saturated vapor enters a tube with a cooled surface, condensation will occur and a thin liquid film will form around the circumference of the tube, resulting in an annular flow pattern. At lower vapor and liquid flow velocities, gravity tends to thicken the condensate layer on the bottom of the tube and a thin layer of condensate exists at the top of the tube. If the vapor flow rate is very high, the condensate is distributed more evenly around the circumference of the tube due to the high vapor shear at the vapor-liquid interface.

The thickness of the liquid film increases as vapor continues to condense. If the liquid and vapor flow rates are relatively low, the effect of gravity becomes important and stratified flow occurs where the condensate collects at the lower portion of the tube in a pool and a thin film of vapor covers the upper portion of the tube. The thick layer of condensate at the bottom of the tube results in a relatively large thermal resistance compared to the top surface of the tube, so condensation primarily occurs through the thin liquid surface on the top of the tube. The flow velocity difference between the vapor core and the condensate layer can cause waves to form at the interface as predicted by the Kelvin-Helmholtz instability theory, and this is called the wavy flow regime. If the liquid and vapor flow velocities are very low, waves will not form and the stratified-smooth flow regime will occur. For wavy flow, when the liquid flow rate is sufficient, the interfacial waves can grow and crest to the top of the tube. This results in the formation of distinct vapor slugs that flow at the top of the tube, and this regime is called slug flow.

The plug flow regime occurs when the large vapor slugs break apart into smaller vapor plugs and bubbles. At very low vapor quality, small bubbles flow at the top of the tube resulting in the bubbly flow regime.

During in-tube condensation of pure fluids, the dominant thermal resistance is due to convection and/or conduction through the liquid condensate on the tube wall. For this reason, successful enhancement techniques will often involve redistributing or mixing of the condensate layer. The microfin surface structure does both of these and also increases the internal surface area. The next section gives an overview of flow pattern visualization studies, flow regime models, and the advances in understanding the heat transfer enhancement mechanisms for condensation in microfin tubes.

2.2 Flow Pattern Observations in Microfin Tubes

Several flow visualization techniques have been used to observe the flow inside microfin tubes. The overarching goal of these studies is to observe the effects of the microfins on the flow of condensate and to explain the mechanisms of heat transfer enhancement. The flow characteristics in a microfin tube are more complex than flow in a smooth tube because of surface tension driven condensate drainage, centrifugal forces that redistribute the condensate, and shear forces that drive condensate downstream within the grooves. From a survey of the literature, some of the flow visualization techniques include using an industrial borescope to take pictures inside a tube (Oh and Bergles, 2002), installing high-speed cameras against sight glasses or other transparent observation sections (Liebenberg and Meyer, 2006), (Liu et al., 2020), (Mohseni and Akhavan-Behabadi, 2011), (Olivier et al., 2007), and using particle image velocimetry to measure flow velocity and turbulent kinetic energy for flows over microfins (Li, Campbell, et al., 2019). Liebenberg and Meyer (2006), in addition to their visual flow observations, analyzed the power spectral density fluctuations of pressure traces for multiple locations along a condensing flow to classify bubbly, slug, and annular flow regimes. Then, they adapted smooth tube flow regime transition criteria to predict flow regimes transitions in microfin tubes. Classifying flow regimes based only on visual observations is subjective, and their study, among others, presents an objective flow regime transition criteria.

Mohseni and Akhavan-Behabadi (2011) visually observed the flow patterns during condensation of R-134a in a 9.52 mm O.D. microfin tube with varying inclination from upward flow, horizontal flow and downward flow. They observed the flow pattern through a smooth sight glass mounted at the end of the test section. The sight glass was 100 mm long and had the same inner diameter as the microfin tube. Experiments were conducted at an average saturation temperature of 35 °C for mass fluxes from 53-212 $\mathrm{kg\,m^{-2}\,s^{-1}}$. Flow pattern maps were produced based on the liquid and vapor Weber numbers, with three separate flow classifications: annular flow, semi-annular flow and stratified flow. Images of the flow pattern were superimposed on each map.

Annular flow was the dominant flow pattern for downward flow, and no flow pattern map was created. This was also the case for downward flow in the tube at $-60°$, except for low mass fluxes and low vapor quality, where stratified flow was observed. For the transition from annular to stratified flow, the condensate flowed mainly at the bottom of the tube and a film of condensate covered the top portion of the tube. Flow regimes in the $-30°$ orientation were similar to the $-60°$ case except for the transition to stratified flow regimes occurred at higher vapor quality.

Condensation in the horizontal tube produced the highest heat transfer coefficients particularly for high vapor quality. Unlike the downward and upward flows, the transitions from annular to wavy-annular, and wavy-annular to stratified-wavy flow were observed in the horizontal tube. They never observed the waves reaching the top side of the sight glass.

For the positive inclinations, the velocity of the condensate was slowed which caused instability and turbulence at the liquid-vapor interface. Compared to downward flow, vertically oriented flows showed similar flow patterns, but turbulence at the interface was more pronounced. Increasing the tube inclination from 30° to 60° caused the transition from annular flow to wavy-annular flow to occur at lower vapor qualities.

They concluded that the fins inside the tube caused an increase in flow turbulence and created swirling flow patterns. The fins also caused mist formation during annular flow which thinned the liquid film around the circumference of the tube leading to enhanced heat transfer. The flow patterns inside the microfin tube were different from those of a plain tube, and new transition criteria were developed for each tube inclination angle.

Colombo et al. (2012) used a visualization chamber to observe condensing flows of R-134a in two microfin tubes and a smooth tube all with 9.52 mm O.D. The microfin tubes had two sets of fins with alternating height, and the fin geometries were similar except for one tube had a total of 54 fins while the other had 82 fins. High-speed videos were recorded and slow motion replay was used to identify the flow characteristics. In the microfin tubes, they observed the transition from annular to intermittent flow occurred at lower quality for a fixed mass flux, and the transition from annular to wavy flow occurred at a lower mass flux for a fixed quality. The delayed transition to intermittent flow was a result of the microfins causing secondary swirling flow patterns, the centrifugal force of the swirling flow, and the capillary force that distributes the condensate all around the perimeter of the tube.

Both of the microfin tubes produced higher heat transfer coefficients than the smooth tube. The microfin tube with 54 fins performed better than the tube with 84 fins at high mass fluxes. The trend of the heat transfer coefficients in the microfin tube with 84 fins tends to flatten at higher mass fluxes, and they expected this tube had too many fins. The enhancement factors for the finned tubes ranged from 1 to 1.5 and were less than the area ratio. Enhancement ratios lower than the surface area ratio indicate the second set of shorter fins may have been relatively ineffective at enhancing heat transfer. The shorter fins will flood with condensate faster than the higher ones making making them less effective. Higher enhancement factors were observed in the tube with fewer fins indicating that a large number of fins decreases enhancement. The penalty factors were similar for both tubes.

Liebenberg and Meyer (2006) condensed R-22, R-407C, and R-134a in 9.5 mm O.D. smooth, microfin and herringbone tubes. Flow regimes were recorded in a transparent sight glass section using a high-speed video camera. Pressure traces were sampled at eight points along the condensing flow path, and frequency and amplitude analyses were performed. The power spectral density distribution of the fluctuating pressure signal was used to objectively identify the prevailing flow regimes. The power spectral density distributions were then compared to the visual flow observations to correlate the harmonic frequencies to certain flow characteristics. The flow regimes observed in the microfin tubes were similar to those for the smooth tube, but the transition from annular flow to intermittent flow occurred at 30-35% vapor quality in the microfin tube while this transition occurred at 48% vapor quality in the smooth tube. Thus, the microfins effectively delay the transition from annular to intermittent flow by 9-18% vapor quality. A new flow regime transition criteria was developed for microfin tubes using the Froude rate parameter and the Martinelli parameter. A distinct swirling swirling flow was observed for the microfin tube that was not observed in the smooth tube. These observations were confirmed by the power spectral density distributions of the microfin tubes.

Oh and Bergles (2002) used an industrial borescope to observe the condensate flow in a smooth tube and four microfin tubes with 9.525 mm O.D. during evaporation and condensation. The microfin tubes had 6°, 18° and 40° spiral angles. The observed liquid distributions around the circumference of the microfin tubes were different than a smooth tube. In some cases the capillary effect and momentum force drove liquid to the top of the microfin tube producing an annular-like flow even when most of the liquid flowed at the bottom of the tube. During condensation at a mass flux of $50\,\mathrm{kg\,m^{-2}\,s^{-1}}$ and a quality of 0.5, they observed that liquid flowed almost continuously to the top of the tube with an 18° spiral angle. Liquid did not flow continuously to the top of the tubes with 6° and 44° spiral angles. The time-averaged wall temperature at the top of the 18° tube was lower than the other tubes and resulted in higher heat transfer coefficients. At a mass flux of $200\,\mathrm{kg\,m^{-2}\,s^{-1}}$, the tube with the 6° spiral angle performed the best because the low spiral angle produced a larger shear force on the liquid flowing in the grooves, leading to enhanced convective heat transfer. At lower mass fluxes and stratified flows, the mechanism of heat transfer enhancement was the increase in wetted surface area on the inside of the microfin tube. At high mass fluxes and annular flows, the mechanism of heat transfer enhancement is due to the high vapor shear that exists on the fin surface which thins the boundary layer and improves convective heat transfer. This effect was best observed in the microfin tube with a 6° helix angle because the vapor flow encountered a gentle slope and would easily flow through the inter-fin region. The steeper slope of the 44° helix angle resulted in a weaker shear force in the interfin region, but the increase in surface area compensated for this and heat transfer coefficients in this tube did not decrease very much compared to the microfin tube with a 6° helix angle. Increasing the helix angle from 6° to 44° increased the pressure drop by a maximum of 10%.

Cavallini, Col, Doretti, et al. (2006) subdivided flow regimes in smooth tubes based on the parameters that influence the condensation heat transfer coefficient rather than the observed flow configuration. Their model is applicable to condensation of halogenated and natural refrigerants, pure fluids and near-azeotropic mixtures in horizontal microfin tubes. Their model accounts for fluid properties, two-phase flow pattern and the geometrical characteristics of the microfin tube. They considered a δT-independent and δT-dependent flow regime with only one transition criterion. The δT-dependent regime represents gravity dominated flow and the δT-independent regime represents shear dominated flow. The transition criterion was obtained from an experimental but objective way from an analysis of condensation heat transfer data. The transition line is modeled using the dimensionless gas velocity, J_G, as a function of the Martinelli parameter, X_{tt}. The transition criterion for condensing refrigerants is shown in Equation 2.3.

$$J_G^T = \left[\left(\frac{7.5}{4.3X_{tt}^{1.111} + 1} \right)^{-3} + 2.6^{-3} \right]^{-1/3} \quad (2.3)$$

Then, this transition criterion is used to calculate the heat transfer coefficient for the δT-dependent and δT-independent flow regimes. The heat transfer coefficient for the δT-independent flow regime, α_A, is calculated using a simple two-phase multiplier to correct the liquid-phase heat transfer coefficient. The heat transfer coefficient for the δT-dependent regime, α_{STRAT}, is calculated by relating α_A to a fully-stratified flow heat transfer coefficient. This correlation method makes for a smooth transition from the wavy-stratified regime to the smooth-stratified regime. The flow regime transition for smooth tubes, shown in Equation 2.3, was modified by Doretti et al. (2013) for application to microfin tubes based on experiments.

Doretti et al. (2013) conducted flow visualization experiments with R-410A, R-134a and R-236ea inside a 7.69 mm I.D. microfin tube and an 8.0 mm I.D. smooth tube. The flow visualization chamber was located at the end of a counter-flow tube-in-tube heat exchanger. A high-speed camera with a macro lens was used to capture images of the flow in the visualization chamber. The visualization chamber was essentially a large sight glass, and the flow at the exit of the smooth or microfin tube was observed. The end of the tube was cut at a 45° angle so the flow inside of the microfin grooves could be observed. The distance between the condensing region of the test section and the visualization chamber was less than 50 mm, so they argued the flow structure was maintained.

For condensation at a 40° saturation temperature, the trends for the enhancement factor against vapor quality were significantly different for mass fluxes of 200, 400, and 800 $\mathrm{kg\,m^{-2}\,s^{-1}}$. The enhancement factors were greatest for the 200 $\mathrm{kg\,m^{-2}\,s^{-1}}$ mass flux and they increased with vapor quality. At 400 $\mathrm{kg\,m^{-2}\,s^{-1}}$, the enhancement factors were near the area enhancement ratio of 1.8, and the trend was fairly flat with respect to the vapor quality. The enhancement factors were below the area enhancement ratio for the highest mass flux of 800 $\mathrm{kg\,m^{-2}\,s^{-1}}$. The different trends for the enhancement factor were explained by comparing the flow regimes in the smooth and microfin tube. Based on the flow regime map proposed by Cavallini, Col, Doretti, et al. (2006) for a smooth tube, stratified flow is expected at a mass flux of 200 $\mathrm{kg\,m^{-2}\,s^{-1}}$, the transition from annular to stratified flow occurs at a mass flux of 400 $\mathrm{kg\,m^{-2}\,s^{-1}}$, and annular flow is expected at a mass flux of 800 $\mathrm{kg\,m^{-2}\,s^{-1}}$. The flow visualization chamber was used to verify the accuracy of the flow regime map proposed by Cavallini, Col, Doretti, et al. (2006). For the microfin tube, the flow at a mass flux of 200 $\mathrm{kg\,m^{-2}\,s^{-1}}$ transitioned from annular to stratified flow, the flow at a mass flux of 400 $\mathrm{kg\,m^{-2}\,s^{-1}}$ appeared to be annular. Annular flow was observed in both tubes at a mass flux of 800 $\mathrm{kg\,m^{-2}\,s^{-1}}$. At lower mass fluxes, annular flow is observed in the microfin tube while stratified flow existed in the smooth tube. The more even distribution of condensate in the microfin tube decreases the thickness of the liquid film on the bottom of the tube and increases heat transfer. Other enhancement effects such as increased turbulence in the liquid film and surface tension driven condensate drainage also contributed to extending the range of annular flow in the microfin tube. They demonstrated the flow regime map proposed by Cavallini, Col, Doretti, et al. (2006) could predict the flow regime transition from shear dominated to gravity dominated flow in a smooth tube, and the modified flow regime transition presented by Doretti et al. (2013) also performed well. The flow regime transition criteria for microfin tube is shown in Equation 2.4.

$$J_G^* = \left[\left(0.6 \frac{7.5}{4.3 X_{tt}^{1.111} + 1} \right)^{-3} + 2.6^{-3} \right]^{-1/3} \tag{2.4}$$

These flow visualization studies have revealed how flow regime transitions in microfin tubes are effected by surface tension driven condensate drainage and the generation of secondary flows. These effects were observed on a macroscopic level, but more insight can be gained by studying these flows in more detail. This is only possible with the help of numerical simulations which are discussed in the next section.

2.3 Numerical Simulations

Bhatia and Webb (2001) numerically simulated sixteen different fin geometries for a 14.9 mm microfin tube. They varied the helix angle, number of fins, fin height, apex angle and top flat width to observe the changes in single-phase friction factor and Nusselt number for a turbulent flow. The greatest error for the numerically calculated friction factor and Nusselt number were 15% and 46%, respectively, compared to the empirical data. They observed that increasing the helix angle increased the Nusselt number and friction factor, but the friction factor increased more than the Nusselt number. The flow started to bypass the interfin region as the helix angle increased resulting in reduced shear stress in the interfin region.

Increasing the number of fins increased the Nusselt number and friction by roughly the same proportion. Increasing the height of the fins from 0.3 to 0.5 mm increased the friction factor by approximately 10%. The Nusselt number increased by 12% when the fin height increased from 0.3 mm to 0.4 mm, and decreased when the fin height was further increased to 0.5 mm. The increase in fin height from 0.4 mm to 0.5 mm reduced the average axial flow velocity in the interfin region by 20% reducing the Nusselt number. Simultaneously, the shear stress at the top of 0.5 mm fins increased and offset the reduction in wall shear stress. Changing the apex angle and profile of the fin top had relatively little effect. Any modification that reduced the interfin cross sectional area produced more flow bypass, reduced the interfin shear stress, and reduced the Nusselt number. The highest shear stresses were observed on the windward fin side near the corner where the side of the fin transitions to the fin top. This numerical study was done for single-phase turbulent flow, but the effects of altering fin geometry on heat transfer and pressure drop can be observed for condensation in finned tubes as well.

Li, Campbell, et al. (2019) used particle image velocimetry and experimental measurements to validate numerical large eddy simulations which were then used to identify the physical mechanisms responsible for heat transfer enhancement in microfin tubes. Experiments and simulations were conducted for single-phase flows of water in the transitional and fully turbulent flows.

The experimental test section had a square cross section that measured 15.2 mm on a side. Both smooth and microfin test sections were constructed. For the microfin tests, only the bottom surface of the test section had a microfin structure and the other walls were smooth. The fins were 0.33 mm in height and had a 45° angle from the stream wise direction.

The numerical simulations revealed that swirling flow was present above the fins when the flow was fully turbulent. In transitional flow, the swirls were less present. They defined two zones to describe fluid mixing in the regions between the fins and above them. The region between the fins was called Zone 1 and the region above the fin tips was Zone 2. The swirls promoted fluid mixing between the two zones which produced higher heat transfer coefficients compared to the smooth surface. Large eddy simulations were used to further explore the effects of swirling flow. The simulations revealed that swirl structures form in the inter-fin region when larger flow structures pass over the fins in Zone 2. The swirls produced in Zone 1 sometimes traveled over the fin and into a downstream fin region.

They also produced contour maps of the thermal boundary layers for the smooth and microfin test sections along the vertical center plane of the flow. For the microfin surface, the temperature sublayers became unstable and the cooler bulk fluid was seen to penetrate through Zone 2 almost to the finned surface. Mixing between the thermal boundary layers increased with Reynolds number and further increased the heat transfer coefficient.

Velocity contours were also shown for the same instance that the swirling flow structures and thermal boundary layers were observed. The velocity gradients were greater near the wall for the microfin surface. This results in greater pressure drop for the microfin surface. The conclusions from this study were the microfins increase the production of coherent structures that enhance fluid mixing between the viscous sublayer and the log-law region just above the fin tips.

Through numerical simulations in ANSYS-CFX, Jasiński (2011) varied the helix angle in a microfin tube from 0° to 90° and used entropy generation minimization analysis to determine the optimum helix angle for a range of Reynolds numbers. Experiments were carried out in a microfin tube with a 30° helix angle, and the results were compared to the numerical simulation for verification. The minimum relative entropy generation rate occurred in a microfin tube with a 70° helix angle. The relative entropy generation rate refers to the ratio of the entropy generated in the microfin tube over a smooth tube, $S'_{gen}/S'_{gen,smooth}$, with the same hydraulic diameter. The minimum entropy generation rate was 33% for the 70° helix angle. An additional result of the numerical study was a map of heat transfer coefficients as they varied over the trough and fin regions. The highest heat transfer coefficients occurred on the tip of the fin specifically on the edges where the side profiles merged with the top profile. The heat transfer coefficient distribution was symmetric for the axial fin case and asymmetric for all other helix angles.

Nozu and Honda (2000) conducted condensation experiments and a numerical analysis of condensation of four different refrigerants in three microfin tubes and a smooth tube. They proposed a correlation for condensation in horizontal microfin tubes based on the results of their numerical analyses, which were confirmed using experimental data from their own study and from the literature. The three microfin tubes had outside diameters ranging from 9.5 to 10.0 mm with varying number of fins, helix angles, and apex angles. The largest heat transfer enhancement was observed for the tube with the largest fin pitch, or in other words, the largest interfin cross sectional flow area. This was due to the rate at which condensate fills the inter-fin region. With more cross sectional area in the interfin region, the grooves can retain condensate to lower vapor quality while still leaving the top of the fin exposed. Two industrial borescopes were used to observe the flow in a microfin tube in the axial direction and from a side view. They defined two flow patterns for the horizontal microfin tubes: at high vapor velocities most of the condensate flowed through the grooves without apparent turbulent mixing in the film and all microfins enhance heat transfer, and for low vapor velocities most of the condensate flowed in the lower portion of the tube and only the upper fins enhance heat transfer. Their numerical investigation focused on determining the effects of fin geometry on the condensate profile along the groove in the annular flow regime. As the vapor quality decreased during condensation, they compared the development of the condensate profile in the interfin region for different microfin geometries. They concluded the flow pattern transition from annular to stratified flow depends on the flow conditions and fin dimensions. Better heat transfer performance was observed in the tube with larger interfin spacing.

2.4 Pure Fluid and Azeotropic Mixture Condensation in Microfin Tubes

Many studies have been conducted for condensation of pure fluids and near-azeotropic mixtures in microfin tubes. Some researchers compare the heat transfer and pressure drop characteristics of an enhanced tube to a similarly sized smooth tube. For comparison, smooth tubes have an inner diameter equal to either the fin tip diameter or the fin root diameter. Many other equivalent smooth tube diameters have been used such as the hydraulic diameter or the fin melt down diameter, but the most common equivalent smooth tube diameter is the fin root diameter. Some studies in the literature are similar to parametric studies where the microfin tube inner diameter remains constant while fin geometries, such as number of fins, fin height, helix angle, fin shape, or apex angle, are varied. Alternatively, researchers have studied multiple microfin tubes with different diameters ranging anywhere from 3 mm to 16 mm for the same range of mass flux and saturation temperature. Lastly, the heat transfer and pressure drop performance of microfin tubes has been compared to cross-grooved tubes and herringbone tubes.

2.4.1 One Microfin Tube

Diani, Brunello, et al. (2020) compared condensation heat transfer for R-513A in a 3.4 mm I.D. microfin tube and a smooth tube with a similar I.D. Heat transfer data were experimentally collected for the smooth and enhanced tube. They found the microfin tube caused an earlier transition to annular flow compared to the smooth tube. As mass velocity increased, the enhancement factor decreased while the pressure gradient increased. They noted that lower mass velocities are recommended for practical use to utilize the maximum heat transfer enhancement while minimizing the increase in pressure gradient.

Diani, Cavallini, et al. (2017) reported experimental condensation heat transfer and pressure drop measurements for R-1234yf inside a 3.4 mm I.D. horizontal microfin tube. Test conditions included saturation temperatures of 30 °C and 40 °C and mass velocities ranging from 100-1000 $\mathrm{kg\,m^{-2}\,s^{-1}}$. All data points were plotted on a flow regime map to distinguish δT-independent and δT-dependent heat transfer regions. The enhancement factor tends to decrease as mass velocity increases indicating the micro fins are advantageous at lower mass velocities. The average enhancement factor was 1.45 and the average penalty factor for pressure drop was 1.24.

Eckels and Tesene (2002) compared the condensation heat transfer and pressure drop performance of R-502 and R-507 in a smooth and microfin tube both with 9.52 mm O.D. The refrigerant R-502 is an azeotropic mixture of R-22 and R-115, and R-507 is an azeotropic blend of R-125 and R-143a. The microfin tube yielded enhancement factors from 1.5 to 2.2 and pressure drop penalty factors from 1.6 to 2. The high enhancement at low qualities was attributed to the microfins delaying the transition from annular to wavy flow.

Diani, Campanale, and Rossetto (2018) experimentally calculated condensation heat transfer coefficient and pressure drop data for R-1234ze(E) and R-134a in a 4.0 mm O.D. microfin tube. Test conditions included saturation temperatures of 30 °C and 40 °C for mass fluxes ranging from 100 to 1000 $\mathrm{kg\,m^{-2}\,s^{-1}}$. R-1234ze(E) had generally higher heat transfer coefficients and pressure drops that were 30% lower compared to R-134a under the same test conditions. R-1234ze(E) has a vapor phase density about 20% lower than R-134a which produces higher vapor phase velocities at the same mass flow rate compared to R-134a. The increased heat transfer coefficients for R-1234ze(E) were attributed to the refrigerant's lower vapor density.

These studies show that the optimum operating conditions for microfin tubes occurs at lower mass fluxes. At low mass fluxes, enhancement factors may range from 120% to 220% and penalty factors may range from 120% to 200% indicating an overall increase in performance for the microfin tubes compared to smooth tubes.

2.4.2 Parametric Studies in Microfin Tubes

Next, the effects of varying fin geometries will be discussed. Khanpara et al. (1986) studied the effect of varying microfin geometries on heat transfer and pressure drop for single-phase and condensing flows with refrigerant R-113. They tested a smooth tube and eight microfin tubes all with 9.52 mm O.D. The geometrical parameters of interest were the peak and valley shape (round or flat), fin height, number of fins, and spiral angle. The maximum enhancement factor observed was 3.83 and pressure drop penalty factors were less than 2. Flat fin peaks and flat valleys resulted in greater enhancement compared to a round shape due to the increased surface area at the fin tip and the increased area in the fin trough region for condensate to drain into. Increasing the fin height caused more surface area to extend past the condensate film and become active in thin-film condensation. After the fins flooded, the fins still disturbed the film and contributed to generating secondary flow patterns. Lastly, they concluded that intermediate spiral angles, around 20°, were more effective than smaller or larger spiral angles.

Graham et al. (1999) condensed R-134a in two grooved tubes: one had axial fins and the second had a 18° helix angle. Both tubes had a 8.91 mm O.D. and a 0.18 mm fin height. At the lowest mass flux of $75\,\mathrm{kg\,m^{-2}\,s^{-1}}$, the spirally finned tube had enhancement factors slightly higher than the 62% increase in the tube's internal surface area, and 20% greater than the axially finned tube. They noted the axial fins may have prevented the condensate from draining to the lower portion of the tube. Comparatively, the helical fins may drain the liquid refrigerant which exposes more surface area for condensation to occur. At higher mass fluxes, both tubes exhibited a trend towards enhancement factors that were less than their smooth tube area ratios. The axially finned tube had higher enhancement factors compared to the helically finned tube for certain ranges of quality when the mass flux ranged from 225-450 $\mathrm{kg\,m^{-2}\,s^{-1}}$. As the mass flux increased, the pronounced enhancement in the axially grooved tube occurred at lower qualities while the enhancement factor in the helically grooved tube remained relatively constant near the level expected due to its area enhancement. The penalty factors for both tubes were very similar for all test conditions.

Bukasa et al. (2004) investigated the influence of the spiral angle on condensation heat transfer for R-22, R-134a and R-407C in microfin tubes with 9.52 mm O.D. A smooth tube and three microfin tubes with 10°, 18° and 37° spiral angles were tested. Heat transfer coefficients increased with spiral angle and the maximum enhancement factor of 2.2 was achieved in the tube with a 37° spiral angle at the lowest mass flux tested ($300\,\mathrm{kg\,m^{-2}\,s^{-1}}$) and at low quality ranging from 0.1 to 0.3. Moderate heat transfer augmentation was observed at moderate vapor quality from

0.4 to 0.9. The larger helix angles redistribute the liquid around the circumference of the tube and the delay the transition to stratified/wavy flow. At high mass fluxes, a moderate heat transfer enhancement was observed over the entire range of vapor quality. In the stratified/wavy flow regime, the microfins reduce the thickness of the condensate layer on the top of the tube, which increases the heat transfer coefficients.

Ishikawa et al. (2002) investigated the effect of the number of fins on condensation heat transfer and pressure drop in horizontal microfin tubes with R-22 as the working fluid. Six helical microfin tubes with 55 to 85 fins were tested while all other fin geometries remained virtually identical. All tubes had 7.56 mm O.D., 0.23 mm fin height and a 16° spiral angle. Heat transfer coefficients were 3.0 to 4.4 times higher in the finned tubes, and the highest heat transfer coefficients were observed in the tube with 80 fins. Heat transfer coefficients increased as the number of fins increased to 80, and no further benefit was observed when the number of fins was increased to 85. The fin trough region becomes narrow and quickly floods with condensate when the fin number is excessively high. There was no distinguishable effect on pressure drop as the number of fins increased from 55 to 85.

Kim and Shin (2005) collected experimental condensation heat transfer data for R-22 and R-410A in seven microfin tubes and one smooth tube all with 9.52 mm O.D. The greatest heat transfer coefficients were observed in the tube with the greatest fin height and therefore largest surface area ratio. It also had the smallest fin apex angle which results in a larger interfin cross-sectional flow area. The outer tube wall temperature was measure on the top, bottom, left and right sides of the tube and the variation in circumferential wall temperature measurements increased as the refrigerant mass flux and quality decreased.

Li, Wu, et al. (2012) investigated condensation heat transfer and pressure drop for R-22 in five helical microfin tubes all with a 5 mm O.D. and an 18° helix angle. The number of fins, apex angle and fin height varied for the tubes. The highest frictional pressure drop was observed in the tube with the largest area ratio and lowest hydraulic diameter. This tube also had the highest heat transfer enhancement factor. The lowest frictional pressure drop was observed in the tube with the lowest fin height, but this tube did not have the lowest area ratio. The tube with the lowest area ratio had the lowest heat transfer enhancement. A non-linear relation between mass flux and heat transfer coefficient was observed and was attributed to the complex interactions of the fins and the fluid. The greatest heat transfer enhancement was observed at low mass fluxes. In addition to the redistribution of condensate by the fins and surface tension drainage, they noted that reduction of the size of turbulent eddies at the wall by the microfins helps enhance heat transfer. Kedzierski and Goncalves (1999) reached a similar conclusion about the reduction in size of the turbulent eddies near the wall.

Cross-grooved and herringbone tubes are both effective heat transfer enhancement techniques. Cross-grooved tubes have a secondary groove cut with the same helix angle as the microfins but in the opposite angular direction. Herringbone tubes have a microfin structure but instead of a helical pattern, they have a chevron pattern where the fins diverge and converge repeatedly. The advantages and disadvantages of these more complex surface structures have been studied and their performance is often compared to helical microfin tubes and smooth tubes. Chamra et al. (1996) compared the condensation performance of single-groove and cross-grooved microfin tubes with 15.88 mm OD and R-22 as the working fluid. The helical microfin tubes and cross-grooved tubes had 74-80 fins, 0.35 mm fin height, and a 30° apex angle. The cross-groove depth was a fraction of the fin height, so the helical structure still remained. They found that the heat transfer enhancement ratio increased from 2.87 to 3.6 in the single-groove tube as the helix angle increased from 15° to 27°, and the penalty factor increased from 1.58 to 2.46. Cross-grooved tubes enhanced heat transfer by about 10% compared to the single-grooved tubes but also increased the pressure drop. The greater heat transfer performance of the cross-grooved tubes was due to the additional surface area created by the cross-grooves, and the increased number of condensate drainage points. Overall, the increase in heat transfer in the cross-grooved tubes was nearly proportional to the increase in pressure drop, so the efficiency index for the two types of microfin tubes was comparable.

Tang et al. (2000) compared the condensation heat transfer performance of R-22, R-134a and the near-azeotropic mixture R-410a in a smooth tube, an axial microfin tube, a helical microfin tube and a cross-grooved helical microfin tube all with 9.52 mm O.D. The cross-grooved geometry is created by cutting a groove with a 40° helix angle into the preexisting axial fins. The groove was cut down to the fin root diameter. Heat transfer enhancement ranged from 60% to 175% for all of the microfin tubes. The cross-grooved tube had the best performance, followed by the axial microfin tube, and then the helical microfin tube. The cross-grooved tube had heat transfer coefficients that were 25% to 45% higher than the helical microfin tube. The increased performance of the cross-grooved tube was attributed to the surface roughness introduced by the cross-cut groove. The axial microfin tube had heat transfer coefficients that were 5 to 10% higher than the helical microfin tube. The axial microfin tube had more fins and a sharper fin apex angle which produced a 19% increase in surface area compared to the helical microfin tube. The increase in performance of the axial microfin tube was attributed to the increase in surface area.

Lambrechts et al. (2006) conducted condensation experiments with R-22, R-134a and R-407C inside a smooth, microfin and herringbone tube all with diameters close to 9.52 mm. The SBG correction factor was used for condensation experiments with R-454C. The greatest enhancement factors were observed for the herringbone with an average enhancement factor of 322% followed by the microfin tube at 196%. The authors attribute heat transfer enhancement in the microfin tube to the secondary swirling flow pattern, surface tension drainage and the increase in surface area. Heat transfer coefficients for the microfin tubes were based on the maximum internal diameter. The microfins delayed the transition from annular to intermittent flow by a vapor quality range of 15-20%. The herringbone tubes perform better and delay the intermittent flow transition by an additional 10-20% vapor quality. In the intermittent flow regime, the main mechanism of heat transfer is through the liquid film at the top of the tube. The authors note that the microfins significantly reduce the thickness of the liquid film which reduces the film conduction resistance.

Liebenberg and Meyer (2008) identified shortcomings in previous models for predicting condensation heat transfer, pressure drop and flow regime transitions in enhanced tubes. For smooth tubes, heat transfer in annular flow is dominated by the viscous base film. The microfins produced re-circulation zones and helical streamlines in the flow direction. These secondary flow patterns promoted vortex shedding and turbulent eddies. A comparison of flow regime transitions for microfin tubes compared to smooth tubes shows that the microfin tubes delay the transition from annular flow to stratified flow. The authors compared heat transfer data for smooth, microfin and herringbone tubes for test conditions at low and high mass flux for refrigerants R-22, R-407C and R-134a. Comparing the data revealed that drop wise condensation is present at very high quality and film wise condensation follows and causes a decrease in heat transfer coefficient. At low mass fluxes, flow in the smooth tube is stratified while the microfin tube redistribute the liquid to an annular flow. Heat transfer enhancement for the microfin and herringbone tubes decreases once the fin tips are submerged in liquid.

They found the increase in pressure drop for microfin tubes is, on average, 1.5 times or less than the smooth tube pressure drop. The pressure drop increases with fin height and helix angle. The pressure drop for herringbone tubes is, on average, 27% greater than a microfin tube. At low mass fluxes, the microfins have little to no effect on the pressure drop. An overall performance factor, or efficiency factor, is used to compare heat transfer enhancement to the increase in pressure drop for the enhanced surface. The authors note that the gain in heat transfer performance compared to the increase in power consumed due to the increase in pressure drop is roughly 1 to 1.

Goto et al. (2001) measured condensation and evaporation heat transfer coefficients and pressure drop for R-410a inside an 8.01 mm O.D. helical microfin tube and an 8.00 mm O.D. herringbone tube. The local heat transfer coefficients were about 1.1 to 1.9 times higher for the herringbone tube compared to the helical microfin tube. They stated the mixing of the thin liquid film at the tips of the herringbone grooves produced the larger heat transfer coefficients at high vapor quality. The same mechanism contributes to heat transfer enhancement in the helical microfin tube. For stratified flow regimes in the helical microfin tube, they noted the helical microfins mix the condensate film and distribute the liquid in the lower portion of the tube and thin the liquid film. They developed a pressure drop correlation that predicted their data to within ±20%.

While some researchers study one microfin tube diameter and vary the fin geometries, others focus on a range of tube diameters. Wu, Sundén, et al. (2014) condensed R-410A in one smooth tube and six microfin tubes with fin root diameters ranging from 4.54 to 8.98 mm. The microfin tubes delayed the transitional vapor quality from annular to intermittent flow by approximately 0.2 compared to the smooth tube. The best heat transfer performance was observed in the tube that had the highest area enhancement, and the lowest performance was observed in the tube with the lowest area enhancement. All tubes had similar heat transfer performance at high mass fluxes ($G \geq 400\,\mathrm{kg\,m^{-2}\,s^{-1}}$). They observed that mass flux had a non-monotonic relation with heat transfer coefficients in the microfin tubes with more significant enhancement occurring at lower mass fluxes.

Han and Lee (2005) conducted condensation experiments with four microfin tubes with 4, 5.1, 6.46 and 8.92 mm O.D. Refrigerants included R-134a, R-22 and R-410a. About 38% of the experimental data were in the stratified wavy flow regime while most of the experimental data for the smaller diameter tubes were in the annular flow regime. The flow pattern in the tube was affected by the geometry of the tube as surface tension and the helix angle extended the annular flow regime compared to a smooth tube. The authors observed an increase in the local penalty factor at high vapor qualities, then after the vapor quality dropped below around 0.6 the local penalty factor decreased. The microfin tubes had a relatively little contribution to turbulence generation in the high vapor quality region, but this becomes more important at intermediate qualities. This phenomenon explains the shape of the penalty factor curve with respect to vapor quality.

The interfin region also floods with liquid faster at higher mass fluxes. Due to interfin flooding and the relative contribution to turbulence generation, the heat transfer enhancement factors were nearly equivalent to the area enhancement ratio for mass fluxes greater than $400\,\mathrm{kg\,m^{-2}\,s^{-1}}$. Additionally, enhancement ratios were less than unity for some test conditions with mass fluxes approximately greater than 800-850 $\mathrm{kg\,m^{-2}\,s^{-1}}$. Enhancement ratios were greater for low mass fluxes for almost all refrigerants in all of the tubes. The enhancement factors were different for each refrigerant and they suggested that each refrigerant may have an optimal tube design.

These parametric studies revealed that intermediate helix angles are most effective for condensation because they effectively redistribute the condensate around the circumference of the tube without an excessive increase in pressure drop. Increasing the number of fins in a tube increases the enhancement factors up to a certain extent. Adding too many fins can reduce enhancement factors because the interfin flow are tends to flood with condensate faster. For this reason, low fin apex angles are favorable to maximize the interfin flow area. Cross-grooved and herringbone tubes have been studied and they produce enhancement factors greater than helical microfin tubes, but they also have larger penalty factors and they are more difficult to manufacture. The enhancement mechanisms that have been cited in the literature are the production of helical streamlines, turbulent eddies and vortex shedding. The fins also mix the liquid-vapor interface at the fin tips. It has also been suggested that microfin tube geometries can be optimized for certain fluids.

2.5 Mixture Condensation in Smooth Tubes

Modeling the condensation process for a multi-component mixture is computationally rigorous due to the coupled heat transfer, mass transfer and fluid mechanics phenomena. At equilibrium, a zeotropic mixture has different compositions in the liquid and vapor phases, as discussed in Chapter 1 of this document. The review by Fronk and Garimella (2013) details the analytical approaches used to model the condensation process for zeotropic mixtures including: conservation equation models, non-equilibrium models, and equilibrium and empirical models. The non-equilibrium film theory approach developed by Colburn and Drew (1937) uses the following assumptions (from Fronk and Garimella (2013)):

1. Concentration and temperature gradients are present in the vapor and liquid phases.

2. Thermodynamic equilibrium is assumed only at the interface.

3. All heat and mass transfer resistance in the vapor phase is confined to a thin film of arbitrary thickness.

4. All heat and mass transfer is in the direction perpendicular to the liquid film.

The non-equilibrium model is a more realistic representation of the mixture condensation process, but it is computationally rigorous and difficult to implement because calculation of the mass transfer in the vapor phase is required. A simplified alternative is the equilibrium approach outlined by Bell and Ghaly (1974). Their method does not consider the mass transfer process directly, but relates the mass transfer resistance to the sensible resistance in the vapor phase. This approach makes the following assumptions:

1. The liquid and vapor phases are in equilibrium at the vapor bulk temperature.

2. The liquid and vapor enthalpies are those of the equilibrium phases at the vapor bulk temperature.

3. The sensible heat of the vapor is transferred from the bulk vapor to the interface by a convective heat transfer process.

4. The total latent heat of condensation and sensible heat of the cooling vapor are transferred through the entire thickness of the liquid film.

The third assumption effectively overestimates the heat transfer resistance in the vapor phase because two-phase heat transfer coefficients are much higher than single-phase heat transfer coefficients. The overestimation of the vapor phase resistance is suggested to compensate for the omitted mass transfer resistance. The mixture heat transfer coefficient calculation is shown in Equation 2.5.

$$\alpha_{mix} = \left[\frac{1}{\alpha_{cond}} + R_{s,v}\right]^{-1} = \left[\frac{1}{\alpha_{cond}} + \frac{\dot{Q}_{s,v}}{\dot{Q}_T}\frac{1}{\alpha_v}\right]^{-1} \tag{2.5}$$

The term α_{cond} is the condensation heat transfer coefficient calculated using a pure fluid correlation, but using the mixture thermophysical properties are used. The term $R_{s,v}$ is the sensible resistance of the vapor. This resistance is calculated using the ratio of the sensible heat removed from the vapor and the total heat removed, $\frac{\dot{Q}_{s,v}}{\dot{Q}_T}$, and the vapor phase heat transfer coefficient, α_v, which is calculated using a single-phase heat transfer correlation applicable for the tube geometry and fluid. The ratio, $\frac{\dot{Q}_{s,v}}{\dot{Q}_T}$, is approximated using Equation 2.6.

$$\frac{\dot{Q}_{s,v}}{\dot{Q}_T} \approx \frac{x\, c_{p,v}\,(T_{dew} - T_{bub})}{h_{lv}} \tag{2.6}$$

Webb, Fahrner, et al. (1996) elaborated on the relationship between the non-equilibrium method and the equilibrium, or Silver and Bell and Ghaly (SBG), method. They compared the heat transfer coefficient predictive capabilities of the two methods. They defined scenarios based on the nondimensional Lewis number where the equilibrium approach is 'safe' to use. The Lewis number, Le, is the ratio of thermal diffusivity over the mass diffusivity. When $Le < 1$, the two methods have decent agreement. When $Le = 1$, the equilibrium method is 'unsafe' in predicting the vapor heat transfer coefficient by up to 50%, and this disagreement gets worse as the Le increases. However, they state the equilibrium method is commonly used in industry and satisfactory condenser performance is a result of an over-sized condenser.

They showed that the non-equilibrium method of Colburn and Drew (1937) predicts condensation rates within 15% while the Bell and Ghaly (1974) approach can under or over-estimate heat transfer coefficients by as much as 150%.

Fronk and Garimella (2016) showed the equilibrium method cannot accurately predict condensation heat transfer coefficients for a mixture with high temperature glide such as ammonia-water. The significant deviations were attributed to the large temperature glide of the mixture. The high glide leads to a large sensible heat load which increases the sensible resistance, $R_{s,v}$ in Equation 2.5.

Jacob and Fronk (2020) condensed the zeotropic refrigerant mixture R-454C in a 4.7 mm I.D. horizontal smooth tube. The experimental heat transfer coefficients for saturation condensation were compared to six correlations from the literature. The correlation developed by Cavallini, Col, Doretti, et al. (2006) performed the best with a MAPE of 6% and 15% with and without the SBG correction, respectively. The SBG correction improved the predictive capabilities of all pure fluid condensation correlations. They concluded the SBG correction was able to accurately predict the saturated condensation for R-454C.

Azzolin et al. (2019) investigated condensation of two azeotropic ternary refrigerant mixtures, R-455A and R-452B, in a minichannel (0.96 mm O.D.) and a conventional tube (8.0 mm O.D.) at similar operating conditions. Condensation tests were conduction at a mean saturation temperature of 40 °C with mass velocities ranging from 100-600 $\mathrm{kg\,m^{-2}\,s^{-1}}$ in the minichannel and 200-800 $\mathrm{kg\,m^{-2}\,s^{-1}}$ in the 8.0 mm tube. Heat transfer coefficients for R-455A were lower that R-452B due to the decreased mass fraction of R-32, which increases the liquid thermal conductivity and latent heat of the mixture. For both mixtures, heat transfer coefficients increase when the difference between the saturation temperature and wall temperature decreases. When the driving temperature difference decreases, concentration gradients in the vapor and liquid phases decrease which reduce the mass transfer resistance. This effect was more apparent at low vapor quality and at low mass fluxes in the larger diameter tube.

Heat transfer performance of the mixtures was compared to their individual pure components. The heat transfer coefficients for R-455A were comparable to R-134yf, but less than R-32 and R-452B. R-452B had higher heat transfer coefficients compared to the R-455A for all of the working conditions in their study. This effect was more pronounced at high vapor qualities. Two-phase frictional pressure gradients were very similar for both mixtures due to their similar liquid viscosity and vapor densities.

2.6 Mixture Condensation in Microfin Tubes

In an early study of zeotropic condensation in finned tubes, Koyama et al. (1990) condensed three binary mixtures of R-22 and R-114, and the individual components in a spirally-grooved tube. The tube had a 9.52 mm O.D., 60 grooves, a groove depth of 0.15 mm, and a spiral angle of 30°. The mixtures consisted of 25, 50, and 75% bulk molar fractions of R-114. Enhancement ratios ranged from 1.4 to 1.7 for R-22, and 1.5 to 1.8 for R-114. The mixture enhancement ratios were lower than those for the pure fluids, and they depended on the bulk concentration and the flow rate of refrigerant. The average heat transfer coefficients were lower for the mixtures with a maximum decrease of 20% compared to the pure components.

In another study, Shizuya et al. (1995) compared the heat transfer enhancement for three binary refrigerant mixtures and all four pure components in a finned tube and a smooth tube both with 7 mm O.D. The fins were 0.19 mm tall, the spiral angle was 14°, and the fin pitch was 0.38 mm. For the binary mixtures, R-22 was mixed with R-142b, R-114 or R-123 as the less volatile component. The less volatile components were selected because their saturation temperatures differ greatly from R-22, and the heat transfer degradation associated with the mixtures would be more pronounced. As the less volatile component condenses, the more volatile component accumulates at the liquid-vapor interface and creates a thick vapor diffusion layer. They stated the fins increased heat transfer in the vapor-diffusion layer and in the liquid film because the fins protrude over the liquid-vapor interface for most of the annular flow regime. Because of this, enhancement ratios for all refrigerants were greater than the inner surface area ratio of 1.6. The heat transfer enhancement compensated for the performance reduction associated with the refrigerant mixtures.

Bukasa et al. (2004) studied the influence of the spiral angle inside microfin tubes during condensation of R-22, R-134a and the zeotropic mixture R-407C. They also included a smooth tube in their experiments. The tubes had 9.52 mm O.D. and spiral angles of 10, 18, and 37°, and all other geometric parameters were held constant. The experimental facility was a vapor compression heat pump and oil concentrations were not directly measured. Heat transfer coefficients increased as the spiral angle increased to 37° and were greater than heat transfer coefficients in the smooth tube for all refrigerants. The authors attributed the heat transfer enhancement to the swirling secondary flow pattern that distributes a liquid film around the circumference of the tube, the surface tension drainage forces at the fin tips, and the mixing at the liquid-vapor interface caused by the fins. Larger helix angles also increase the internal surface area. Enhancement factors were largest for the lowest mass flux of $300\,\mathrm{kg\,m^{-2}\,s^{-1}}$ and lowest for the highest mass flux of $800\,\mathrm{kg\,m^{-2}\,s^{-1}}$. During low mass flux conditions, intermittent flow was present for vapor quality less than 30%. In this regime, heat transfer enhancement was due to the thinning of the liquid film on the top of the tube. Enhancement is less effective at high vapor quality, but the microfins may mix the liquid-vapor interface since the liquid film is very thin.

Shizuya et al. (1995) compared the condensation performance of four pure refrigerants, R-22, R-142b, R-114, and R-123, and three binary mixtures of R-22 with the previously listed refrigerants in smooth and helically grooved tubes with a 7 mm O.D. For the R-22/114 mixture, heat transfer was approximately equal to or slightly higher than the average of the pure components in both smooth and grooved tubes. For the R-22/114 and R-22/123 mixtures, heat transfer was lower inside the smooth tube, but approximately equal to or slightly higher than the average of the pure components inside the grooved tube. They concluded that grooving the inside surface of the tube compensates to a large degree for the degradation of heat transfer performance for the mixtures. The enhancement factors for all fluids exceeded the surface area ratio of 1.6. They attributed the enhanced heat transfer performance to the fins protruding over the liquid film for most of the annular flow regime, which enhanced heat transfer in the vapor diffusion layer as well as in the liquid film.

Eckels and Tesene (1999a) experimentally determined heat transfer coefficients for R-22, R-134a, R-410a and R-407C in one 9.52 mm O.D. smooth and microfin tube, and a 7.94 mm and 15.88 mm O.D. microfin tube. Saturation temperatures were varied from 40 to 50 °C and mass fluxes ranged from 125 to 600 $\mathrm{kg\,m^{-2}\,s^{-1}}$. Heat transfer coefficients were greater in the microfin tubes for all refrigerants at all test conditions. R-134a had the highest heat transfer coefficients in both tubes while R-407C had the lowest heat transfer coefficients in both tubes. The greatest enhancement factors were observed at low refrigerant mass fluxes. The microfin tube more than doubled the heat transfer coefficients at low mass fluxes with enhancement factors from 2.2 to 2.5. At the lowest mass flux, enhancement factors varied from 1.2 to 1.6. They attributed the enhancement at lower flow rates to the fins enhancing turbulence in the condensate layer and delaying the transition from annular flow to stratified flow. For the highest mass flux tested, they observed greater enhancement at lower vapor quality. Heat transfer coefficients were increased by about 50% for all refrigerants. In the second part of their investigation, they reported that pressure drop in the microfin tubes increased by 40% to 80% for all refrigerants compared to the smooth tube (Eckels and Tesene, 1999b).

Kondou et al. (2015) investigated condensation of R-32 and R-1234ze(E), binary mixtures of R-32/R-1234ze(E) and ternary mixtures of R-744/R-32/R-1234ze(E) in a 6 mm O.D. horizontal microfin tube. Two different mass compositions were tested for both the binary mixture and the ternary mixture. The pressure gradient for condensation of the binary mixture decreased with increasing circulation composition of R-32. Increasing the mass fraction of R-32 increases the vapor phase density which reduced the vapor velocity. Single-component correlations were used to predict pressure gradients for the binary and ternary mixtures, and showed good agreement with the experimental data. The correlation of Cavallini, Del Col, Mancin, et al. (2009) with the correction method of Bell and Ghaly (1974) predicted heat transfer coefficients with good agreement. Experimental heat transfer coefficients deviated from predicted values at vapor qualities greater than 0.7, as noted by Cavallini, Censi, Del Col, et al. (2001) and Cavallini, Del Col, Mancin, et al. (2009). Heat transfer coefficients were lower for the binary and ternary mixtures compared to their pure components, and the ternary mixture had the lowest heat transfer coefficients. The ternary mixture of R-744/32/1234ze(E) with the highest temperature glide (18.7 K) had the lowest heat transfer coefficients compared to all other binary and ternary mixtures in their study. Increasing the mass flux beyond $350\,\mathrm{kg\,m^{-2}\,s^{-1}}$ mitigated the mass transfer resistance of the mixtures. This effect was caused by the thinning of the concentration boundary layer that occurred at higher refrigerant flow speeds. They noted the critical mass flux at which this effects occurs should depend on the magnitude of the volatility difference for the mixture's components.

Smit et al. (2002) investigated how condensation heat transfer coefficients are affected by changing the mass fraction of a binary refrigerant mixture. Refrigerant R-142b was added to R-22 and experiments were conducted ranging from 100% R-22 to 50/50% R-22/R-142b in 10% mass fraction increments. Condensation tests were conducted using a smooth tube with a 9.53 mm outer diameter over a range of mass fluxes from 40-800 $\mathrm{kg\,m^{-2}\,s^{-1}}$. In general, heat transfer coefficients decreased as the mass fraction of R-142b increased. They found that condensation heat transfer coefficients were more dependent on the mass fraction of R-142b at lower mass fluxes compared to higher mass fluxes. At low mass fluxes, from 40 to 350 $\mathrm{kg\,m^{-2}\,s^{-1}}$, heat transfer coefficients decreased by as much as 33% as the mass fraction of R-142b increased. For mass fluxes greater than 350 $\mathrm{kg\,m^{-2}\,s^{-1}}$, the flow regime was annular and the heat transfer coefficients were not as strongly affected by the mixture mass fraction, decreasing by only 7%. Heat transfer coefficients decreased as the The transition from annular to wavy flow also occurred at greater vapor quality as more R-142b was added to the mixture.

Jung et al. (2004) measured condensation heat transfer coefficients for R-22, R-134a, R-407C and R-410A inside smooth and microfin tubes with 9.52 mm O.D. R-407C is a zeotropic mixture with a 6 °C temperature glide. The microfin tube had 60 fins, a 0.2 mm fin height and a 18° helix angle. Experiments were carried out at conditions similar to those encountered in residential air conditioners. Heat transfer enhancement factors for the microfin tube ranged from 2-3. Heat transfer coefficients for R-134a were similar to those of R-22 while heat transfer coefficients for R-410A and R-407C were 23-53% and 10-21% lower than those for R-22, respectively. They attributed the degradation of heat transfer for R-410A and R-407C to their lower liquid density and surface tension compared to R-22 which led to a thicker condensate film over the fin tips. Heat transfer coefficients for R-407C were lower than R-410A because it has a greater temperature glide. For R-407C in the smooth and microfin tube, the heat transfer coefficients increased with quality and mass flux. This result indicated the mass transfer resistance was dampened due to the increase in flow turbulence, and the heat transfer coefficients for R-407C increased more rapidly compared to other refrigerants. The enhancement factors for R-22 and R-134a were larger than those for R-410A and R-407C because the microfin structure was optimized for R-22. A redesigned tube could improve the performance of R-407C and R-410A.

Cavallini, Censi, Col, et al. (2002) compared the heat transfer performance of R-134a and the zeotropic mixture R-407C in a smooth tube and a microfin tube with 9.5 mm O.D. under the same operating conditions. For R-134a, the highest enhancement factor was 2.8 which occurred at a saturation temperature of 40 °C and a mass flux of $200\,\mathrm{kg\,m^{-2}\,s^{-1}}$. The surface area ratio of the microfin tube was 1.8. Enhancement factors decreased as mass flux increased, and the enhancement factor at the highest mass flux of $800\,\mathrm{kg\,m^{-2}\,s^{-1}}$ was lower than the surface area ratio. Heat transfer coefficients for R-407C were 15% to 25% lower compared to R-134a at the same operating conditions. The heat transfer enhancement created by the grooves and the degradation associated with the zeotropic mixture both depended on the mass velocity.

Patil (2012) conducted a performance analysis of a vapor-compression refrigeration system for two shell and tube condensers, one with a smooth tube and one with a microfin tube. The hydrofluorocarbon (HFC) refrigerant blend R-404A flowed in the tube-side. The microfin tube condenser improved cooling capacity for the system by 10% and COP by 17% relative to the smooth tube condenser.

A summary of experimental operating conditions and microfin tube outer diameters from the literature are summarized in Table 2.1. This summary does not include all internal condensation experiments in microfin tubes, however it shows that experimental data is sparse for next-generation zeotropic mixtures in smaller diameter tubes. A visual representation of these studies is given in Figure 2.1. Figure 2.2 shows the condensation studies in microfin tubes for zeotropic mixtures only. It is clear there is a lack of experimental data for condensation of zeotropic mixtures in small diameter microfin tubes, and this work addresses this gap.

Table 2.1: Experimental operating conditions for internal condensation in microfin tubes

Reference	**Fluid**	$\mathbf{T_{sat}}$ [°C]	**x** [-]	**G** [$\mathrm{kg\,m^{-2}\,s^{-1}}$]	**D** [mm]	$\mathbf{n_g}$ [-]	**h** [mm]	β [°]
Koyama et al. (1990)	22, 114, 22/114	36-54	0-1	130-360	8.32	60	0.15	30
Khanpara et al. (1986)	113	86-90	0.15-0.85	197-594	9.52	60-70	0.10-0.19	
Shizuya et al. (1995)	22/142b, 22/114, 22/123	47-77	0.02-0.9	188-738	7	49	0.19	14
Chamra et al. (1996)	22	24	0.2-0.8	45-181	15.88	74-80	0.35	30
Eckels and Tesene (1999a)	22, 134a, 410a, 407c	40, 50	0.05-0.95	125-600	7.94-15.88	50, 60	8-12	18, 27
Kedzierski and Goncalves (1999)	134a, 410a, 125, 32	22-51	0-1	85-500	9.5	60	0.2	18
Graham et al. (1999)	134a	35	0.09-0.81	75-450	9.52	60	0.18	0
Tang et al. (2000)	22, 134a,410a	40.6	0.02-0.98	250-810	9.52	60	0.2	18
Cavallini, Censi, Col, et al. (2002)	134a, 407C	40, 55	0.18-0.82	100-800	9.5	60	0.23	13
Eckels and Tesene (2002)	502, 507	40, 50	0.06-0.84	120-600	9.52	60	0.203	18
Ishikawa et al. (2002)	22	45	0-1	160-320	7	55-85	0.21-0.24	16
Infante Ferreira et al. (2003)	404A	40	0-1	200-600	9.52	54	0.16-0.21	15
Jung et al. (2004)	22, 134a, 407C, 410A	40	0-1	100-300	9.52	60	0.2	18
Bukasa et al. (2004)	22, 134a, 407C	40	0.1-0.9	300-800	9.52	60	0.182-0.229	10-37
Han and Lee (2005)	134a, 22, 410A	18.5-33.8	0.18-0.86	91-1110	4-8.92	60	0.11-0.15	beta
Kim and Shin (2005)	22, 410A	45	0.1-0.9	183-365	9.52	54-65	0.12-0.25	15.5-30
Cavallini, Col, Mancin, et al. (2006)	410A	40	0.2-0.8	100-800	7.69	60	0.23	13
Li, Wu, et al. (2012)	22	47	0.1-0.8	200-650	5	35-58	0.10-0.15	18
Colombo et al. (2012)	134a	35	0.10-0.75	100-440	9.52	54, 82	0.16-0.23	0.18
Wu, Sundén, et al. (2014)	410A	39-47	0.1-0.8	99-603	4.56-8.98	35-70	0.10-0.16	18
Diani, Campanale, Cavallini, et al. (2018)	1234yf, 1234ze(E)	30, 40	0.2-0.95	300-1000	3	40	0.12	7
Hirose et al. (2018)	32, 152a, 410a	35	0-0.95	100-400	4	40	0.18	17
Kondou (2019)	1123/32	40	0.1-1	200-400	6	30	0.269	18
Adelaja et al. (2019)	134a	40	0.1-0.9	200-600	9.55	60	0.21	14
Diani, Brunello, et al. (2020)	513A	30, 40	0.1-0.99	100-1000	4	40	0.12	18
Bashar et al. (2020)	1234yf	20, 30	0-1	50-200	2.5	25	0.10	10

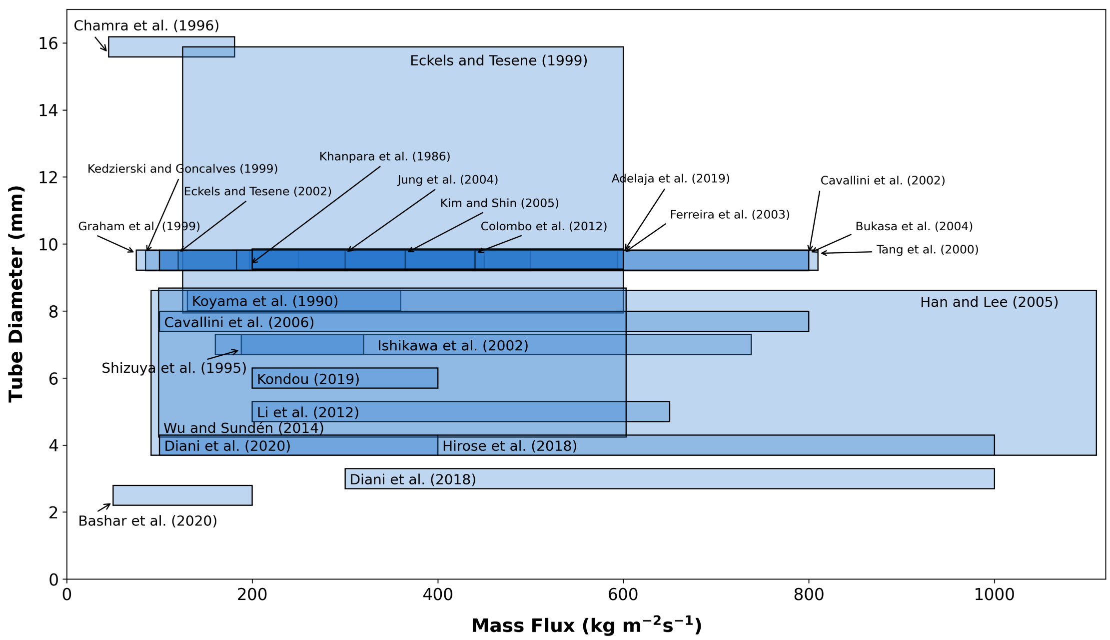

Figure 2.1: A visual representation of operating conditions from the literature for condensation studies in microfin tubes.

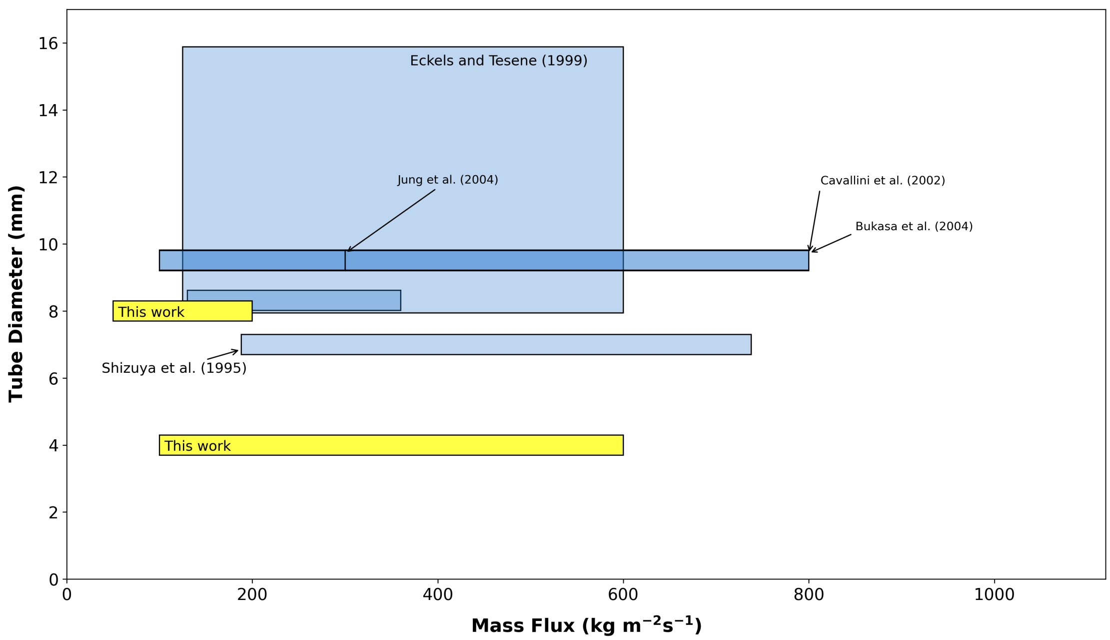

Figure 2.2: Operating conditions for condensation of zeotropic mixtures in microfin tubes.

Chapter 3: Materials and Methods

This chapter provides details on the experimental facility used in this investigation, including its design and operation, measurements, experimental uncertainty, and the methods used to calculate heat transfer coefficients and frictional pressure drop from experimental data.

3.1 Experimental Facility

The experimental condensation facility, shown as a schematic in Figure 3.1, was designed to measure heat transfer coefficients and frictional pressure drop for condensation of a refrigerant. A photo of the test facility showing the test section and various components of the water and refrigerants loops is shown in Figure 3.2.

The experimental facility consists of a refrigerant loop and a water loop. The refrigerant loop consists of a positive-displacement gear pump, an evaporator, the test section, and a post-cooler. The refrigerant pump is magnetically coupled to the drive motor, so no lubricating oil is present in the loop. The refrigerant mass flow rate is measured using a Coriolis-effect mass flow meter. Liquid refrigerant is pumped to the evaporator section where the refrigerant is vaporized and superheated using three 2300 W cartridge heaters. The power input to the evaporator section is controlled using a silicon controlled rectifier (SCR). The superheated vapor, shown

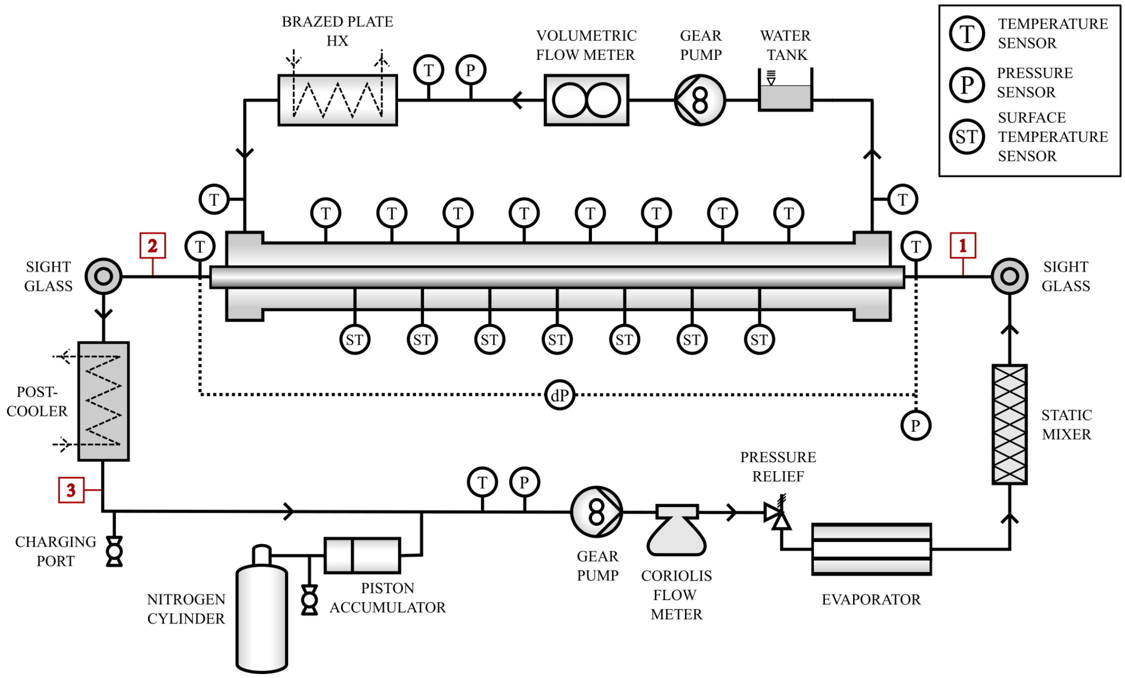

Figure 3.1: A schematic of the experimental facility.

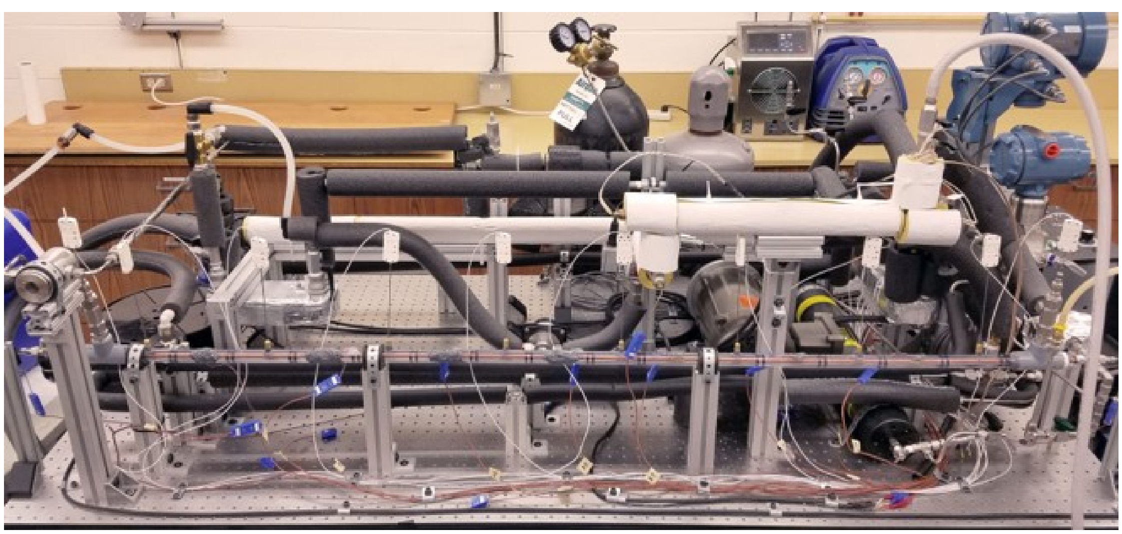

Figure 3.2: A photo of the experimental test facility.

as state point 1 in Figure 3.1, then enters the test section which is a counter-flow tube-in-tube heat exchanger. Deionized water is the secondary cooling fluid in the test section and flows in the annulus. The refrigerant condenses along the length of the test section and exits as a subcooled liquid, shown as state point 2 in Figure 3.1. Sight glasses at the inlet and outlet of the test section provide visual verification that the refrigerant is superheated at the inlet and subcooled at the outlet. A ethylene-glycol coupled post-cooler is installed after the test section to ensure vapor does not flow to the pump during start-up and shut-down procedures. At state point 3 in Figure 3.1, the refrigerant exits the post-cooler as a subcooled liquid, and the liquid refrigerant flows back to the gear pump. The system pressure in the refrigerant loop is set using a piston accumulator and a nitrogen cylinder.

The water loop consists of an open reservoir, positive displacement gear pump, and a brazed plate heat exchanger. The flow rate of water is measured using a positive displacement volumetric flow meter. The water flow rate is controlled using a DC variable speed drive connected to a power supply. The mass flow rate of water through the test section is calculated using the volumetric flow rate and the density of water at the pump outlet, calculated from the measured temperature and pressure. Before the water enters the test section, it is cooled in a brazed plate heat exchanger. The cooling fluid in the brazed plate heat exchanger is an ethylene-glycol solution that is recirculated by a chiller.

Prior to this work, the test facility was used by Jacob, Matty, et al. (2019), Jacob, Matty, et al. (2020) and Jacob and Fronk (2020) to conduct condensation experiments in smooth tubes. Several validation experiments were conducted to gain confidence in the proper operation of all components and sensors in the test facility. These included single-phase liquid and vapor pressure drop tests, energy balance tests, and pure fluid condensation tests. The energy balance test proved the accuracy of the measured water volumetric flow rate, inlet and outlet temperatures, and the refrigerant mass flow rate. The differences in heat duties for the refrigerant and water were less than 1.2% on average. Condensation experiments with R-134a proved the measured local heat transfer coefficients and frictional pressure drops were in good agreement with correlations from the literature. Validation tests were also carried out prior to this study and they are discussed in Chapter 4.

3.1.1 Test Section

The test section is a counter flow, tube-in-tube heat exchanger with water flowing in the annulus and refrigerant flowing in the inner microfin tube. The outer tube is made of PVC, and its diameter varies depending on the diameter of the microfin tube. A rendering of the test section is shown in Figure 3.3. Temperature and pressure measurements from the test section are used to calculate quasi-local heat transfer coefficients and frictional pressure drop for complete condensation. The temperature and pressure measurements are described below.

Resistance temperature detectors (RTDs) are spaced evenly over the length of the test section, and they are inserted midway into the annular gap to measure the axial water temperature along the test section. The RTDs divide the test section into segments, and each segment is approximately 19 cm long for the 4 mm microfin

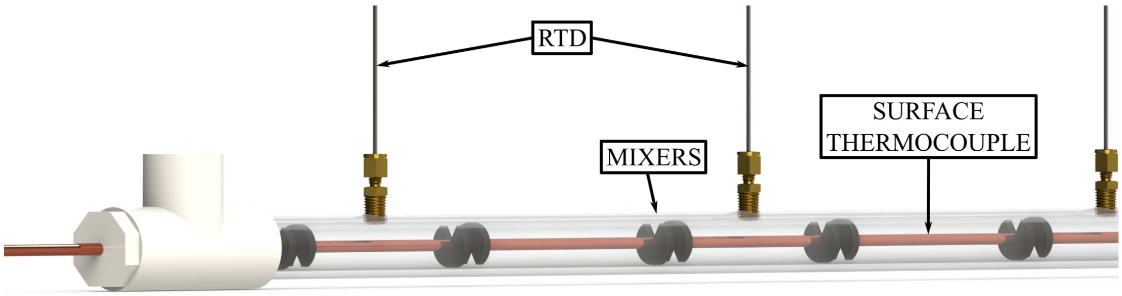

Figure 3.3: A rendering of the test section showing the location of RTDs, flow mixers, and surface temperature measurements.

test section and 17 cm long for the 8 mm microfin test section. A quasi-local heat transfer coefficient is calculated for each one of these segments.

Flow mixers are positioned before and after each RTD to ensure the bulk water temperature is measured. Two additional RTDs measure the water temperature at the inlet and outlet of the test section. Two T-type thermocouples measure the inlet and outlet temperature of the refrigerant. Fine-gauge, bare-bead, T-type thermocouples were soldered to the surface of the microfin tube at the middle of each segment to measure the outer surface temperature. For the 4 mm OD microfin tube, surface temperature measurements were taken on the top side of the tube only. For the 8 mm OD microfin tube, surface temperature measurements were recorded on the top, bottom, left, and right sides of the tube. More surface temperature measurements were installed on the larger diameter tube because flow stratification was expected at the lower mass fluxes of interest.

The 4 mm O.D. microfin tube has a wall thickness of 0.18 mm, a 0.12 mm fin height, 22° helix angle, 42° apex angle and 36 fins. The area ratio for this tube is

1.56. The 8 mm O.D. microfin tube has a 0.25 mm wall thickness, a 0.2 mm fin height, 18° helix angle, 42° apex angle and 50 fins. The area ratio for the 8 mm microfin tube is 1.62.

The surface area ratio is defined as the actual inner surface area of the microfin tube over the inner surface area of a smooth tube with the same inner diameter, D_i, and is calculated using Equation (3.1) from (Webb and Kim, 2005). The surface area ratio is 1.56 and 1.62 for the 4 mm and 8 mm microfin tubes, respectively.

$$\frac{A}{A_p} = 1 + 2\frac{h}{p}\left[\sec\left(\frac{\gamma}{2}\right) - \tan\left(\frac{\gamma}{2}\right)\right] \tag{3.1}$$

3.1.2 Refrigerant Charging Procedure

A consistent refrigerant charging and recovery procedure was used to mitigate refrigerant cross-contamination and trapping of non-condensable gases in the experimental facility. A vacuum pump was used to remove air from the refrigerant loop, refrigerant hoses, and other pipe connections before charging the system. The vacuum pump was left on until a vacuum of 100 microns (0.013 kPa) or less was achieved.

A liquid refrigerant charging procedure was always used. For refrigerant tanks with a Y-valve and dip tube, the liquid port was opened to charge the system. For refrigerant tanks without a Y-valve, the tank was inverted to provide an all-liquid charge.

To change the refrigerant, a refrigerant recovery machine was used to remove all liquid and vapor refrigerant from the facility and store it in a recovery cylinder. After recovering the refrigerant, the vacuum pump was used to pull a vacuum to the tolerance listed above, and the liquid charging procedure was used to introduce the new refrigerant. This process eliminated the possibility of refrigerant cross-contamination, and also ensured no refrigerant escaped to the atmosphere.

3.2 Data reduction

The data reduction procedures for calculating condensation heat transfer coefficients and frictional pressure drop will be discussed in the following sections. Experimental uncertainty for the temperature and pressure measurements, and the uncertainty propagation for the calculated heat transfer coefficients and frictional pressure drop will also be discussed.

The system was allowed to reach a steady state before collecting a data set. Steady state was achieved when temperature, absolute pressure, differential pressure, and mass flow rate readings varied less than 0.1 °C, 10 kPa, 0.1 kPa, and $0.1\,\mathrm{g\,s^{-1}}$ over a four-minute period. Data were collected for a four-minute period at a sampling rate of 4 Hz. The time-averaged values for temperatures, pressures, and flow rates were used for calculations. Data processing was carried out using Engineering Equation Solver (Klein and Nellis, 2020) with refrigerant property data from REFPROP 10 (Lemmon et al., 2018).

3.2.1 Heat Transfer Coefficients

As previously mentioned, the test section is divided into segments by the location of the RTDs. Water-side energy balances are used in each segment to determine the segment heat duty. The heat duty in each segment, Q_i, is calculated using Equation (3.2), where $\dot{m}_w$ is the water mass flow rate, $c_{p,w}$ is the specific heat of water evaluated at the average temperature for a segment, and $\Delta T_{w,i}$ is the change in water temperature for a segment. The heat gained by the water is assumed to be the same as the heat lost by the refrigerant. The average difference between the heat gained by the water and the heat rejected by the refrigerant was 1.7% with a maximum deviation of 6.6%. At the refrigerant inlet of the test section, the refrigerant is superheated and the enthalpy is evaluated using the temperature, pressure and bulk composition of the refrigerant. Water side energy balances are used to determine the refrigerant enthalpy for each subsequent segment in the test section. The refrigerant enthalpy, h_r, at the outlet of each segment is calculated using Equation (3.3), where $\dot{m}_r$ is the refrigerant mass flow rate. The subscript i indicates the segment number. The heat flux, $\dot{q}''$, for a segment is calculated using Equation (3.4), where D_i is the tube diameter to the fin root. This assumes a constant heat flux in each segment.

$$\dot{q}_i = \dot{m}_w \, c_{p,w} \, \Delta T_{w,i} \tag{3.2}$$

$$h_{r,out,i} = h_{r,in,i} - \frac{\dot{q}_i}{\dot{m}_r} \tag{3.3}$$

$$\dot{q}'' = \frac{\dot{q}}{\pi\, D_i\, L} \tag{3.4}$$

The inner wall temperature, $T_{wall,in}$, of the microfin tube is calculated using Equation (3.5), which is the one-dimensional heat conduction equation utilizing the measured outer wall temperature, $T_{wall,out}$. L_i is the length of a segment and k_c is the conductivity of copper. Axial conduction is neglected as 99.9% of the total heat is transferred in the direction normal to the tube surface as demonstrated by Jacob (2020) for condensation in a 4.7 mm smooth tube.

$$T_{wall,in,i} = T_{wall,out,i} + \frac{\dot{q}_i \ln \frac{D_o}{D_i}}{2\pi L_i k_c} \tag{3.5}$$

The heat transfer coefficient is calculated as shown in Equation (3.6) where $T_{r,sat}$ is the equilibrium saturation temperature of the refrigerant at the system pressure. For low-temperature glide mixtures, such as R-454C, the interface temperature can be approximated as the equilibrium saturation temperature with reasonable accuracy (Fronk and Garimella, 2013).

$$\alpha_i = \frac{\dot{q}''}{T_{r,sat} - T_{wall,in,i}} \tag{3.6}$$

The vapour quality at the inlet and outlet of each segment is evaluated using REFPROP 10 (Lemmon et al., 2018) with the known system pressure and refrigerant enthalpy for each segment. For each segment, the average of the inlet and outlet quality is used for comparison with other data points.

3.2.2 Two-phase Frictional Pressure Drop

The differential pressure transducer ports were installed at the inlet and outlet of the test section as shown in Figure 3.1. The measured pressure gradient for complete condensation, ΔP_m, includes the pressure change due to deceleration of the condensed refrigerant, ΔP_d, the frictional pressure drop, ΔP_{fr}, and the pressure drop due to single-phase flow regions at the inlet of the test section, $\Delta P_{fr,v}$, and outlet of the test section,$\Delta P_{fr,l}$. The frictional pressure gradient is calculated as shown in Equation (3.7).

$$\Delta P_{fr} = \Delta P_m + \Delta P_d - \Delta P_{fr,v} - \Delta P_{fr,l} \tag{3.7}$$

The flow deceleration contribution to the overall pressure gradient is evaluated using Equation (3.8), where $\rho_{r,v}$ and $\rho_{r,l}$ are the vapor and liquid phase densities, respectively.

$$\Delta P_d = \rho_v V_v^2 - \rho_l V_l^2 \tag{3.8}$$

The length of the two-phase flow region in the test section was determined by fitting a second-order polynomial to the vapor quality and the corresponding axial position along the microfin tube, as described in (Jacob, Matty, et al., 2019). The physical location where condensation started and ended was determined by evaluating the polynomial at vapor qualities of 1 and 0, respectively. The lengths over which single-phase vapor and liquid flows occurred were estimated using the known length of the microfin tube between the two differential pressure ports. The single-phase frictional pressure drops were evaluated using a correlation by Ravigururajan and Bergles (1996) developed for single-phase flow in microfin tubes. The hydraulic diameter of the microfin tube was used in this correlation rather than the maximum inside diameter as suggested by Wu and Sundén (2016). Single-phase experiments were conducted prior to this investigation to verify the accuracy of the modification proposed by Wu and Sundén (2016). The correlation predicted experimental single-phase frictional pressure drops with a mean absolute percentage error (MAPE) of 7% for Reynolds numbers from 2,500 to 30,000.

The correlation developed by Wu and Sundén (2016) modified a correlation developed by Ravigururajan and Bergles (1996) to account for the additional roughness created by the microfins on the inner surface of the tube. The modification consisted of using the Churchill model to include roughness effects introduced by the microfins on the inner surface of the tube, and also using the hydraulic diameter of the microfin tube rather the fin root diameter (Wu and Sundén, 2016).

3.2.3 Uncertainty Analysis and Calibration

The surface temperatures of the microfin tube are measured using T-type thermocouples that have an uncertainty of $\pm 0.5\,^{\circ}\mathrm{C}$ as specified by the manufacturer. The refrigerant inlet and outlet temperatures were also measured using T-type thermocouples and had the same uncertainty. The measurement ranges and systematic uncertainties for all measurements are shown in Table 3.1.

Table 3.1: Instrument ranges and uncertainties

Measurement	**Range**	**Systematic Uncertainty**
RTD	-200 - 500 °C	±0.05 °C
Surface temperature	-40 - 260 °C	±0.5 °C
T-type thermocouple	-40 - 260 °C	±0.5 °C
Pressure	0 - 10 MPa	±5.68 kPa
Differential pressure	0 - 249 MPa	±0.05 kPa
Refrigerant mass flow meter	0 - 30 $\mathrm{g\,s^{-1}}$	±0.1 %
Water volumetric flow meter	0.04 - 7.5 $\mathrm{L\,min^{-1}}$	±0.5 %

Uncertainties in the calculated frictional pressure drop and heat transfer coefficients were calculated using an uncertainty propagation analysis suggested by Kline and McClintock (1953). The uncertainty in the calculated variables is due to systematic and random uncertainties from the temperature, pressure, flow meters and the data acquisition system. Systematic uncertainties, shown in Table 3.1, were evaluated based on the uncertainty of the sensor, data acquisition system and the calibration process.

The largest source of uncertainty in calculating heat transfer coefficients was from the measured water temperature profile. The temperature change of water in an individual segment of the test section can be fairly small, typically around 1 to 2 °C, and was used to determine the heat duty for each segment. The RTDs were calibrated using a temperature bath and a high-accuracy reference temperature probe to reduce the uncertainty of the calculated heat transfer coefficients. The uncertainty specified by the manufacturer for the RTDs was ±0.15 °C at 0 °C. The temperature bath has a temperature stability and uniformity of 0.01 °C and 0.02 °C. The reference temperature probe had an uncertainty of ±0.012 °C at 0 °C.

The RTDs were calibrated using four temperature data points from 5 to 40 °C. For each calibration data point, data were collected for four minutes using the DAQ and LabVIEW software. This eliminated systematic errors introduced by the DAQ. The measurements from the RTDs were compared to the reference probe and corrected in LabVIEW. After applying the corrections, the calibration was checked by letting the temperature bath stabilize at an intermediate temperature and comparing the measured temperatures to the reference probe once again.

The uncertainty after the calibration process is due to uncertainty contributions from the reference probe, and the stability and uniformity of the temperature bath, as shown in Equation 3.9.

$$U_{sys,RTD} = \sqrt{U_p^2 + U_{bath,s}^2 + U_{bath,u}^2 + U_{error}^2} \tag{3.9}$$

The U_{error}^2 term is the maximum difference of the temperature measured by the reference probe and the RTDs. The resulting systematic uncertainty for the RTDs was less than 0.05 °C, so a conservative uncertainty of 0.05 °C was applied for all uncertainty propagation calculations in this study.

Chapter 4: Results and Discussion

Heat transfer and pressure drop results are presented in this chapter along with details of the initial facility validation. Condensation experiments were conducted for the zeotropic refrigerant mixture R-454C and its individual components R-1234yf and R-32.

4.1 Facility Validation

Prior to collecting condensation data for this study, a validation procedure ensured all components and sensors were working properly. Validation experiments were conducted with R-134a as the working fluid because its heat transfer and pressure drop characteristics have been studied extensively (Kedzierski and Goncalves, 1999), (Cavallini, Del Col, Mancin, et al., 2009), (Eckels and Tesene, 1999a). The validation process included the following tests:

- Single-phase liquid pressure drop tests
- Pure fluid condensation tests
- Energy balance tests

Single-phase liquid pressure drop tests were conducted with R-134a to verify the accuracy of the differential pressure transducer. The single-phase frictional pressure

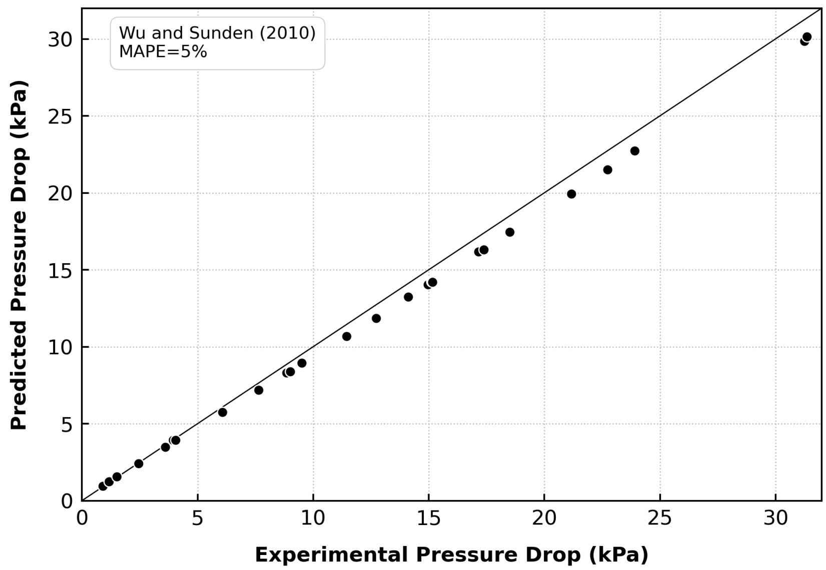

Figure 4.1: Experimentally measured single-phase frictional pressure gradients compared to those predicted by the Wu and Sundén (2016) correlation.

drops were evaluated using a correlation by Ravigururajan and Bergles (1996) developed for single-phase flow in microfin tubes. The hydraulic diameter of the microfin tube was used in this correlation rather than the maximum inside diameter as suggested by Wu and Sundén (2016). A total of 27 data points were collected, and the Wu and Sundén (2016) correlation predicted experimental single-phase frictional pressure drops with a MAPE of 5% for Reynolds numbers from 4,570 to 30,816. The agreement between the predicted and measured pressure drop values was quantified by evaluating the MAPE as shown in Equation 4.1.

$$MAPE = \frac{100\%}{n} \sum_{n=1}^{n} \frac{|P_{predicted} - P_{measured}|}{P_{measured}} \tag{4.1}$$

Condensation heat transfer experiments were also conducted with R-134a for

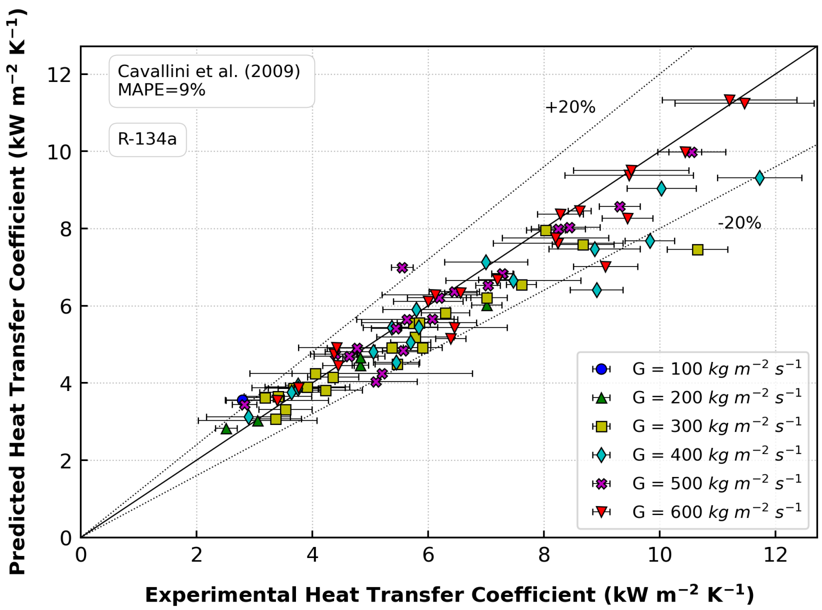

Figure 4.2: Experimental condensation heat transfer coefficients for R-134a compared to the correlation developed by Cavallini, Del Col, Mancin, et al. (2009).

mass fluxes from 100 to 600 $\mathrm{kg\,m^{-2}\,s^{-1}}$ at saturation temperatures of 40, 50 and 60 °C. The heat transfer results were compared to multiple microfin heat transfer correlations, and the correlation developed by Cavallini, Del Col, Mancin, et al. (2009) performed the best with a MAPE of 7%, as shown in Figure 4.2. An energy balance was used to compare the heat gained by the water to the heat rejected by the refrigerant. The differences in heat duties were less than 0.9% on average, and the maximum difference was 2.5%.

The two-phase frictional pressure drop was calculated for the condensation tests. The experimental results were compared to the correlation developed by Cavallini, Del Col, Longo, et al. (1997), as shown in Figure 4.3. The correlation predicted the experimental data with a MAPE of 25%.

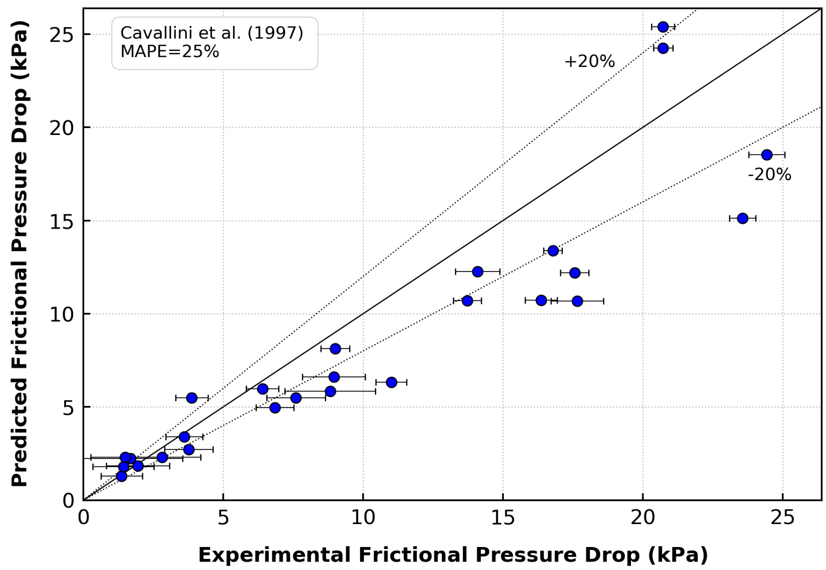

Figure 4.3: Experimental condensation frictional pressure drops for R-134a compared to the correlation developed by Cavallini, Del Col, Longo, et al. (1997).

The heat transfer and pressure drop results with R-134a verified the measurement techniques and operation of the experimental facility. This facility was used to investigate condensation of the zeotropic mixture R-454C and its components, R-32 and R-1234yf, in two microfin tubes with similar test sections.

4.2 Experimental Matrix

Table 4.1 shows the experimental data collection matrix for this study. Heat transfer and pressure drop data were obtained for R-32 at a saturation temperature of 40 °C for mass fluxes from 100 to 500 $\mathrm{kg\,m^{-2}\,s^{-1}}$ due to pressure limitations of the test facility. R-1234yf was not tested in the 8 mm O.D. microfin tube.

Table 4.1: Experimental test matrix

O.D. (mm)	Fluid	$T_{sat,avg}$ (°C)	Mass flux (kg m^{-2} s^{-1}) 50	100	200	300	400	500	600
4	R-454C,	40		x	x	x	x	x	x
	R-1234yf	50		x	x	x	x	x	x
		60		x	x	x	x	x	x
4	R-32	40		x	x	x	x	x	
8	R-454C,	40	x	x	x				
	R-1234yf	50	x	x	x				
		60	x	x	x				
8	R-32	40	x	x	x				

4.3 Heat Transfer Coefficients

The microfin flow regime map proposed by Doretti et al. (2013) is shown in Figures 4.4 and 4.5 for the 4 mm and 8 mm microfin tubes, respectively. Experimental condensation data points for R-454C are overlaid on each plot. The flow regime transition line for smooth tubes, originally proposed by Cavallini, Col, Doretti, et al. (2006), is plotted as a solid line and the modified microfin transition line is plotted as a dashed line. On the flow regime maps, the transition from annular flow to wavy-stratified flow in the microfin tube occurs at a lower dimensionless gas velocity, J_G, compared to the smooth tube as observed by Oh and Bergles (2002), Liebenberg and Meyer (2006), Doretti et al. (2013), and Mohseni and Akhavan-Behabadi (2011). For the 4 mm microfin tube, the majority of the flow patterns fall in the annular regime, and the transition to stratified flow only occurs for the lowest mass flux tested of $100\,\mathrm{kg\,m^{-2}\,s^{-1}}$. In the annular regime, the condensate will be distributed more evenly around the circumference of the tube. In contrast,

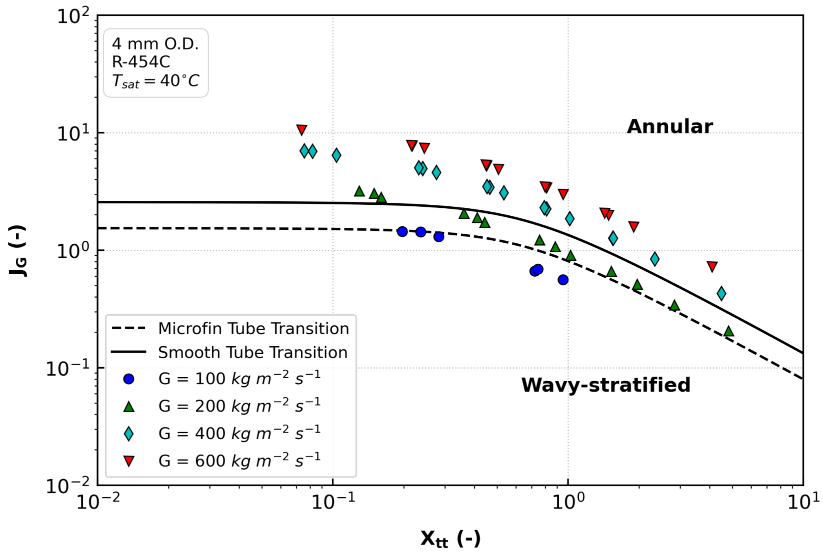

Figure 4.4: Experimental data points for condensing R-454C in the 4 mm microfin tube plotted on the flow regime map proposed by Doretti et al. (2013).

the dominant flow regime in the 8 mm microfin tube is stratified-wavy flow. The transition from annular to wavy-stratified flow occurs for the highest mass flux tested of $200\,\mathrm{kg\,m^{-2}\,s^{-1}}$, and fully stratified flow is expected for all lower mass fluxes. In the stratified regime, condensate collects at the bottom of the tube and vapor condenses on the upper portion of the tube.

For annular flow, it is possible to predict the vapor quality at which the interfin region becomes flooded with condensate if it is assumed that the condensate is perfectly distributed around the circumference of the tube. Prior to flooding, the fins protrude through the annular film and drain condensate from the tips of the fins to the interfin region. More importantly for the mixture, the fins protrude past the liquid-vapor interface and the mass transfer resistance is mitigated. Webb and Kim (2005) outlined the procedure for predicting the vapor quality at which the

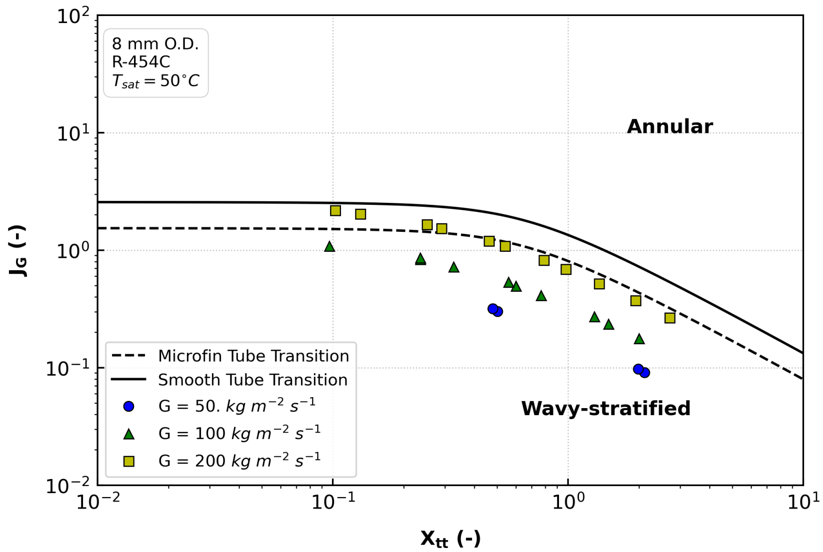

Figure 4.5: Experimental data points for condensing R-454C in the 8 mm microfin tube plotted on the flow regime map proposed by Doretti et al. (2013).

fins become flooded with condensate. First, the cross-sectional area of the interfin region must be known. For the 4 mm microfin tube, the interfin cross sectional area is approximately 9.4% of the total flow area while it is 6.6% for the 8 mm microfin tube. If the void fraction is less than 90.6% or 94.4% for the 4 mm and 8 mm tube, respectively, then the fins will be flooded with condensate. The void fraction correlation by Zivi (1964) is used to estimate the vapor quality that will result in a void fraction of 90.6% or 94.4%. The vapor quality at on the onset of flooding, x_{fill}, is shown in Figure 4.6. The cross-sectional area of the interfin region is a larger fraction of the total flow area for the smaller diameter microfin tube so x_{fill} is lower for the smaller diameter tube. As the saturation temperature increases, x_{fill} increases because the liquid phase density increases. The less dense liquid causes the interfin region to flood at higher vapor quality. To summarize,

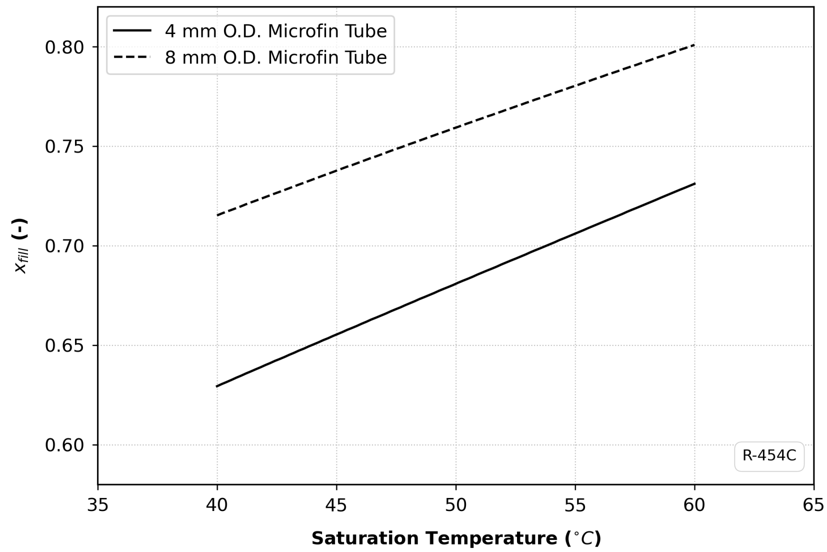

Figure 4.6: Predicted vapor quality at which the interfin region becomes flooded with condensate for R-454C in both microfin tubes.

most of the experimental condensation data in the 4 mm microfin tube is in the annular flow regime and most of the data is in the wavy-stratified flow regime for the 8 mm microfin tube. Additionally, the fins flood with condensate in the 4 mm microfin tube at a lower vapor quality compared to the larger 8 mm microfin tube.

4.3.1 Heat Transfer Coefficients in the 4 mm O.D. Microfin Tube

The measured heat transfer coefficients for R-454C are plotted against vapor quality for average saturation temperatures of 40, 50, and 60 °C in Figure 4.7. Generally, the heat transfer coefficients tend to increase with quality and mass flux, and decrease with increasing average saturation temperature. These trends are also observed for R-32 and R-1234yf in Figures 4.8 and 4.9. R-32 has the highest heat transfer coefficients of the three refrigerants, as shown in Figure 4.8, due to its high liquid thermal conductivity.

The enhancement factors for R-454C, R-32 and R-1234yf are shown in Figure 4.10. To calculate the enhancement factor, the smooth tube diameter in this investigation is the root diameter of the microfin tube and the smooth tube heat transfer coefficients are calculated using a correlation developed by Cavallini, Col, Mancin, et al. (2006). The enhancement factors are only shown for condensation at a saturation temperature of 40 °C, or the average saturation temperature for R-454C. The enhancement factors tend to increase with vapor quality. This trend is observed because as the vapor quality decreases, the inter-fin region fills with condensate, and eventually the condensate layer rises above the fins and the inter-fin region remains flooded. Before the onset of flooding, the fins drain condensate from the fin tip to the trough region leaving a thin layer of condensate at the tip of the fin. The thinner layer of condensate results in a reduced thermal resistance between the cooled surface and the bulk flow which produces high heat transfer coefficients.

However, the enhancement factors do not always increase with mass flux as the heat transfer coefficients do. Figure 4.11 shows the enhancement factors plotted against the mass flux for R-454C, R-32 and R-1234yf at a saturation temperature of 40 °C. It becomes clear that the enhancement factors increase with mass flux up to around $200\,\mathrm{kg\,m^{-2}\,s^{-1}}$ and then they decrease as the mass flux increases to $600\,\mathrm{kg\,m^{-2}\,s^{-1}}$. This trend holds for all three refrigerants in the 4 mm O.D. microfin tube. Pronounced enhancement at low mass fluxes is due to the redistribution of condensate around the circumference of the tube, surface tension driven drainage

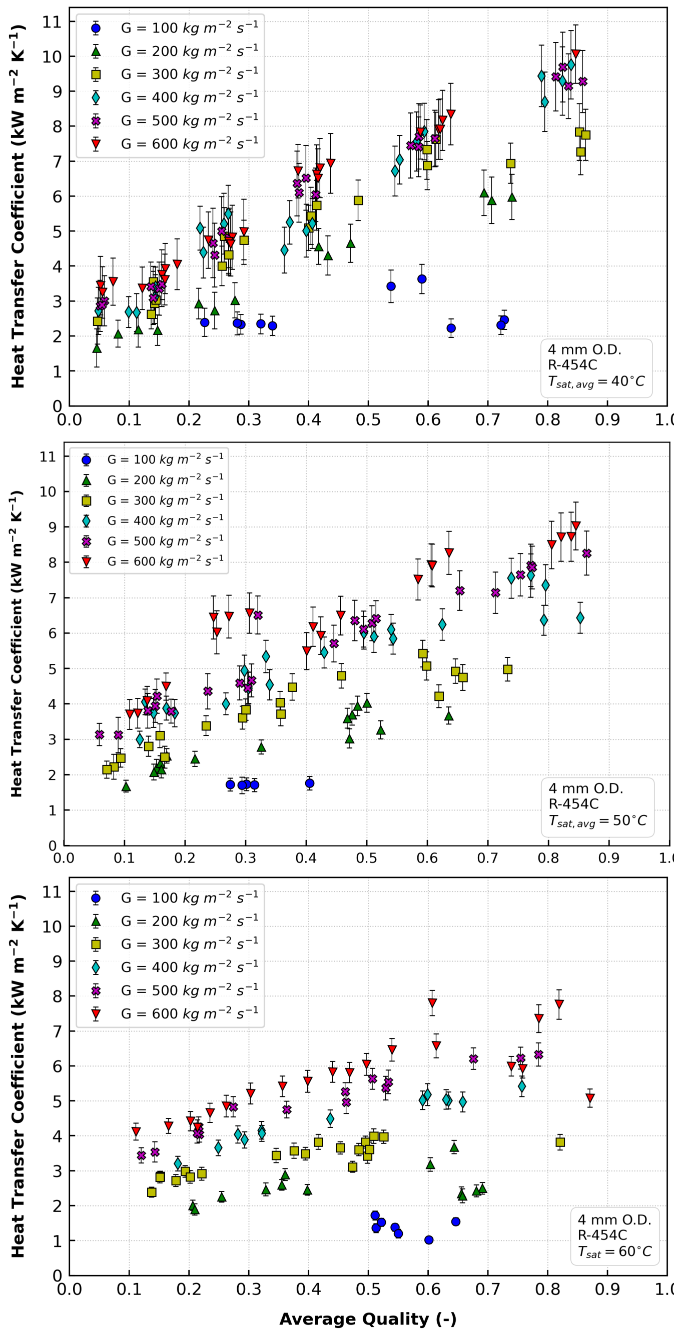

Figure 4.7: Heat transfer coefficients versus thermodynamic quality for R-454C condensing at $T_{sat,avg} = 40, 50$ and $60\,^{\circ}$C in the 4 mm microfin tube.

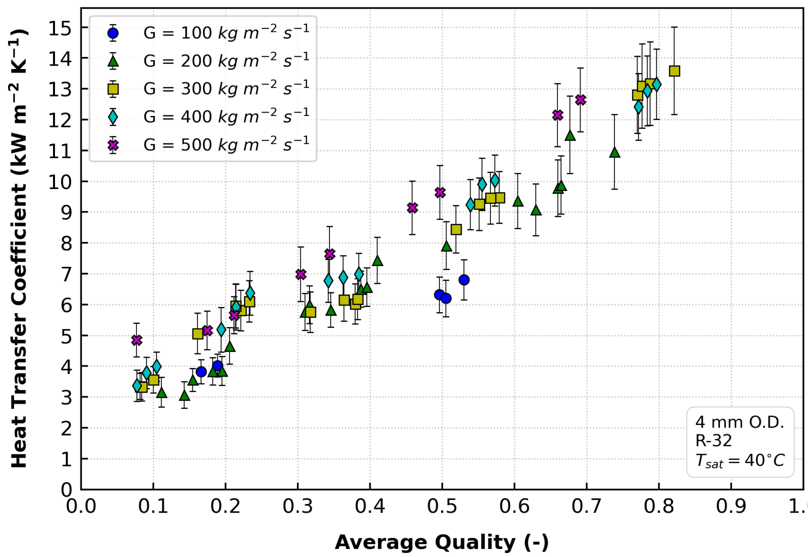

Figure 4.8: Heat transfer coefficients versus thermodynamic quality for R-32 condensing at $T_{sat} = 40\,^{\circ}\mathrm{C}$.

from the fin tips to the trough region, and the increased interfacial turbulence caused by the fins (Wu, Sundén, et al., 2014). Kedzierski and Goncalves (1999) attributed the enhancement at low mass fluxes to the reduction in size of the turbulent eddies at the wall which is caused by the fins.

The measured heat transfer coefficients for the pure fluids are compared to the microfin condensation heat transfer correlations developed by Cavallini, Del Col, Mancin, et al. (2009), Kedzierski and Goncalves (1999) and Yu and Koyama (1998) in Figure 4.12. These correlations were developed for modeling pure fluid or near-azeotropic mixture condensation. The Cavallini, Del Col, Mancin, et al. (2009) correlation performed the best with a MAPE of 17%.

The measured heat transfer coefficients for R-454C are also compared to these

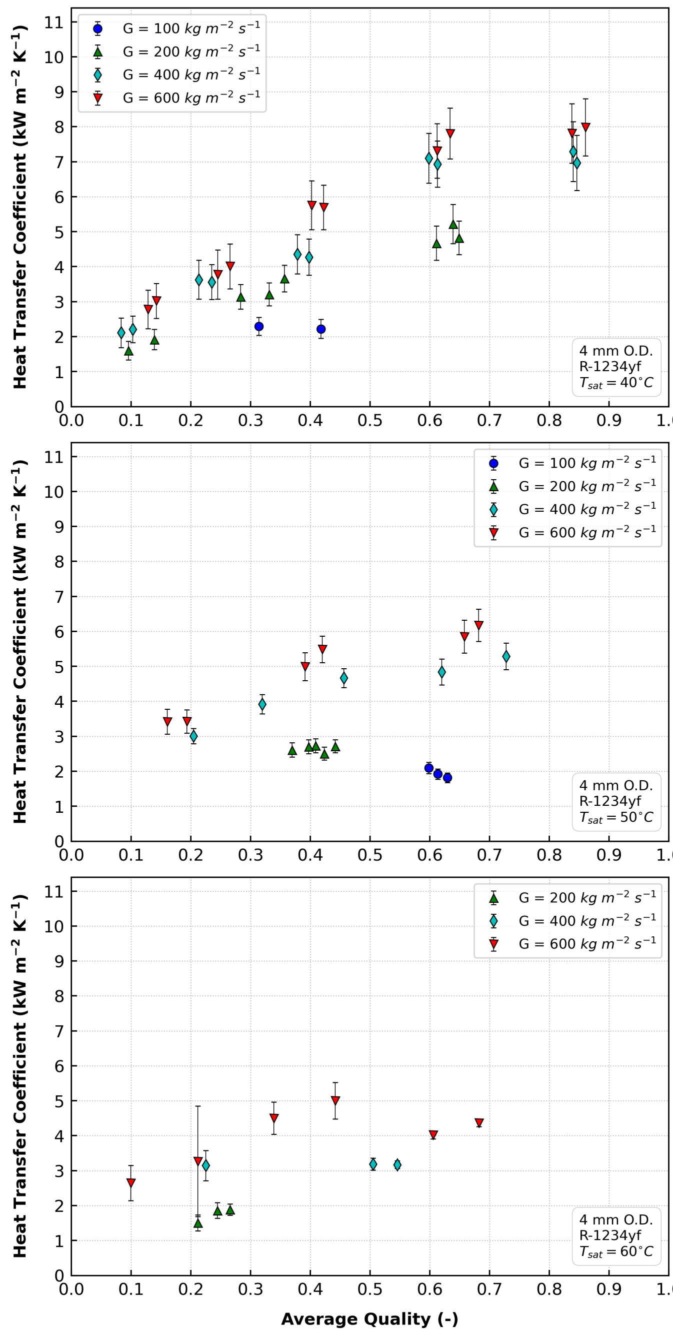

Figure 4.9: Heat transfer coefficients versus thermodynamic quality for R-1234yf condensing at $T_{sat} = 40, 50$ and $60\,^{\circ}$C.

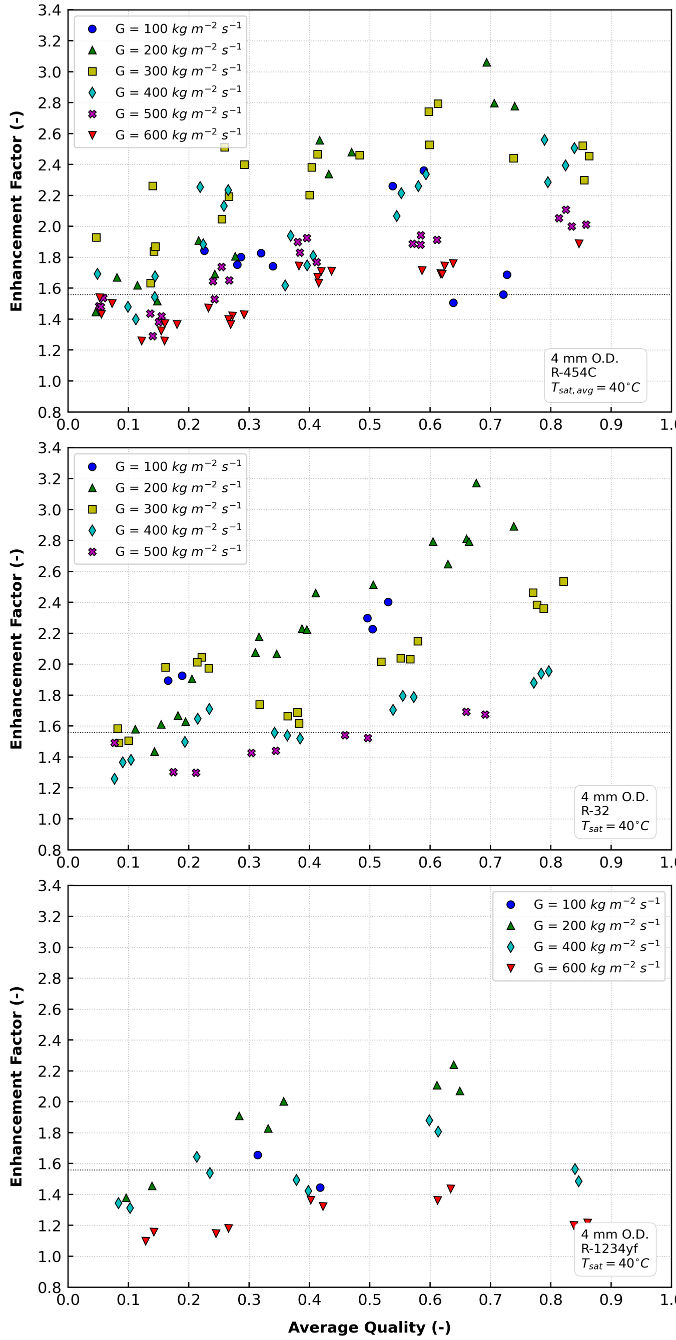

Figure 4.10: Enhancement factors for R-454C, R-32 and R-1234yf at $T_{sat} = 40\,^{\circ}\mathrm{C}$.

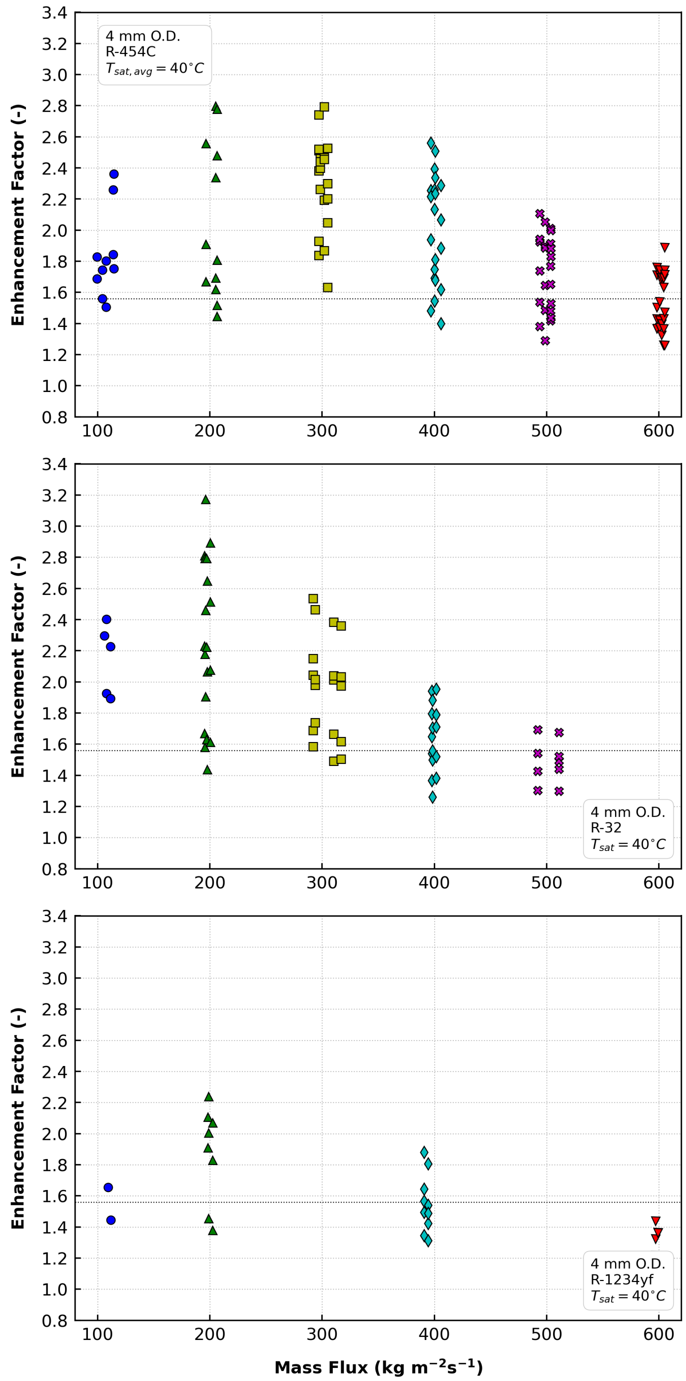

Figure 4.11: Enhancement factors versus mass flux for R-454C, R-32 and R-1234yf at $T_{sat} = 40\,^{\circ}\mathrm{C}$.

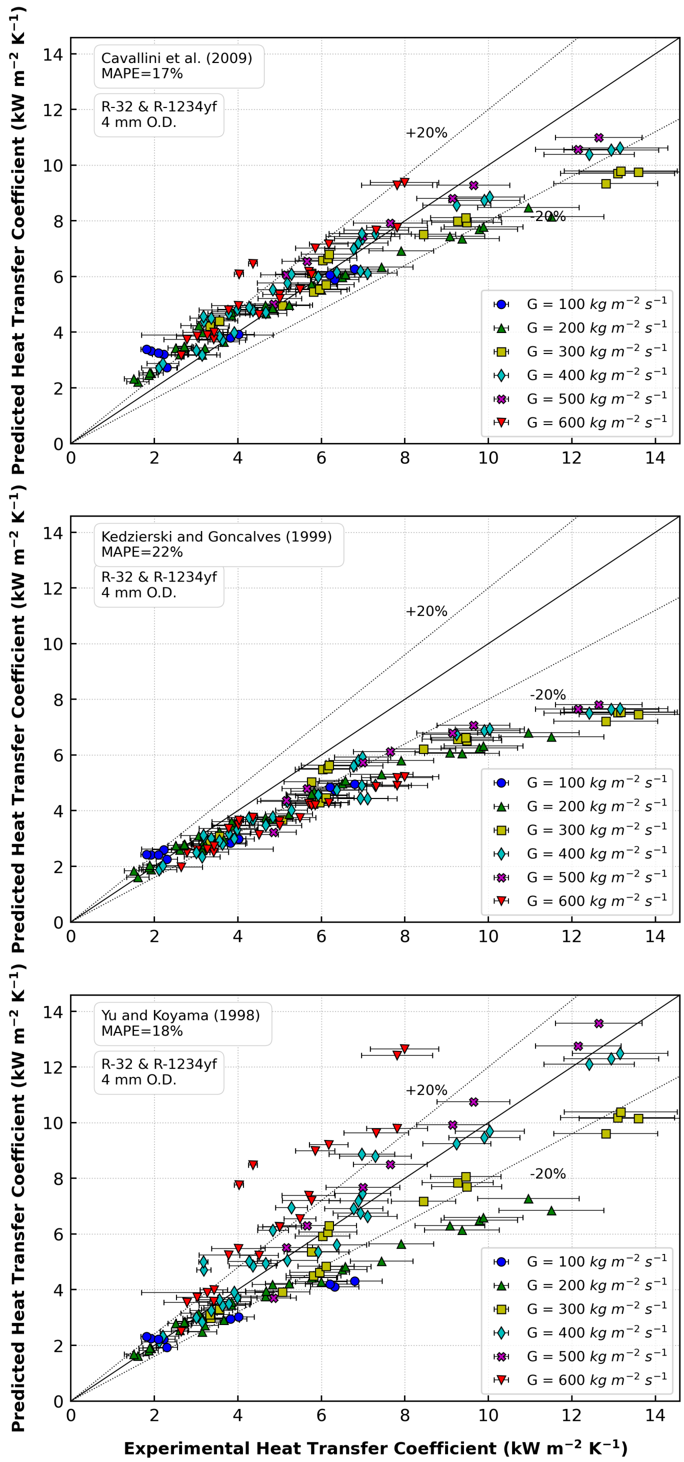

Figure 4.12: A comparison of measured heat transfer coefficients for R-32 and R-1234yf against pure fluid heat transfer correlations from the literature.

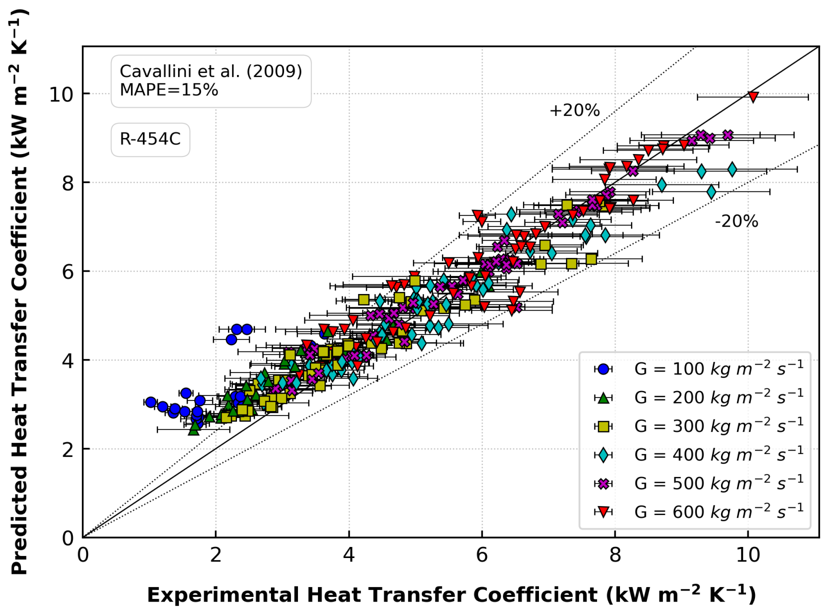

Figure 4.13: A comparison of measured heat transfer coefficients for R-454C against the Cavallini, Del Col, Mancin, et al. (2009) heat transfer correlation.

same correlations both with and without the Bell and Ghaly (1974), or SBG, correction. For the 4 mm O.D. microfin tube specifically, the agreement between the correlations and experimental data is better without the SBG correction. The correlations by Cavallini, Del Col, Mancin, et al. (2009) and Yu and Koyama (1998) performed equally well with a MAPE of 15%. The SBG correction reduced the MAPE of the Cavallini, Del Col, Mancin, et al. (2009) correlation and the Yu and Koyama (1998) correlation by 5% and 8%, respectively. This result suggests that the additional mass transfer and sensible resistances are mitigated by the effects of the microfins. The increased flow mixing between the vapor bulk and condensate, and the effects of condensate drainage must counteract the additional resistances present during mixture condensation.

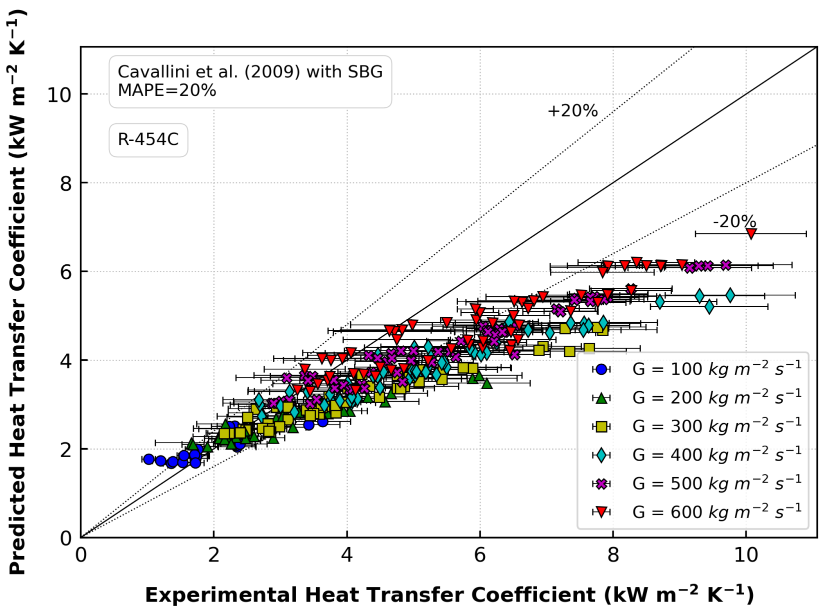

Figure 4.14: A comparison of measured heat transfer coefficients for R-454C against the Cavallini, Del Col, Mancin, et al. (2009) heat transfer correlation with the Bell and Ghaly (1974) correction applied.

4.3.2 Heat Transfer Coefficients in the 8 mm O.D. Microfin Tube

Condensation experiments were also carried out in an 8 mm O.D. microfin tube. The experimental heat transfer coefficients for condensing R-454C at average saturation temperatures of 40, 50 and 60 °C are shown in Figure 4.15, and the heat transfer coefficients for R-32 are shown in Figure 4.16. The heat transfer coefficients increase with vapor quality and with mass flux, as expected. For R-32, the heat transfer coefficients at mass fluxes of 50 and 100 $\mathrm{kg\,m^{-2}\,s^{-1}}$ are very similar.

The enhancement factors for R-454C and R-32 are plotted against vapor quality in Figure 4.17 and 4.18, respectively. The enhancement factors increase with vapor quality for both fluids as they did in the 4 mm microfin tube, but the effect of increasing the mass flux is less evident due to the lower range of mass fluxes tested. The enhancement factors for R-454C and R-32 are plotted against the mass flux in Figures 4.19 and 4.20, respectively. Figure 4.19 shows the maximum enhancement factor for R-454C is 2.5 and occurs at a mass flux of 200 $\mathrm{kg\,m^{-2}\,s^{-1}}$. Similar to the 4 mm microfin tube, most of enhancement factors in the 8 mm microfin tube are greater than the surface area ratio as indicated by the horizontal dashed line. Figure 4.20 shows the maximum enhancement factors at 50 and 100 $\mathrm{kg\,m^{-2}\,s^{-1}}$ are almost identical. The maximum enhancement factors in the 8 mm microfin tube are generally less than the maximum enhancement factors in the 4 mm microfin tube at the same mass flux. Without experimental data at a 300 $\mathrm{kg\,m^{-2}\,s^{-1}}$ mass flux, it is not clear if the highest enhancement factors occur at a mass flux of 200 $\mathrm{kg\,m^{-2}\,s^{-1}}$. The increase in enhancement factor from 100 to 200 $\mathrm{kg\,m^{-2}\,s^{-1}}$ is

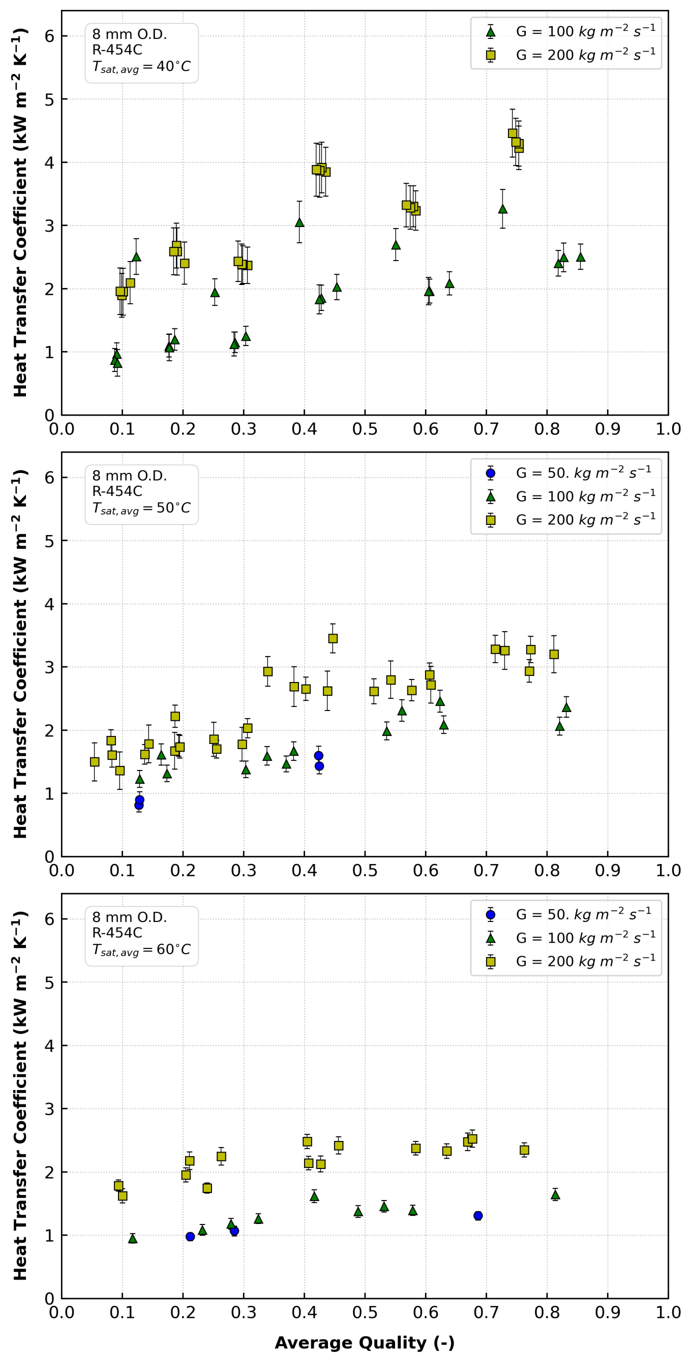

Figure 4.15: Heat transfer coefficients versus thermodynamic quality for R-454C condensing at $T_{sat,avg} = 40, 50$ and $60\,°\mathrm{C}$ in the 8 mm microfin tube.

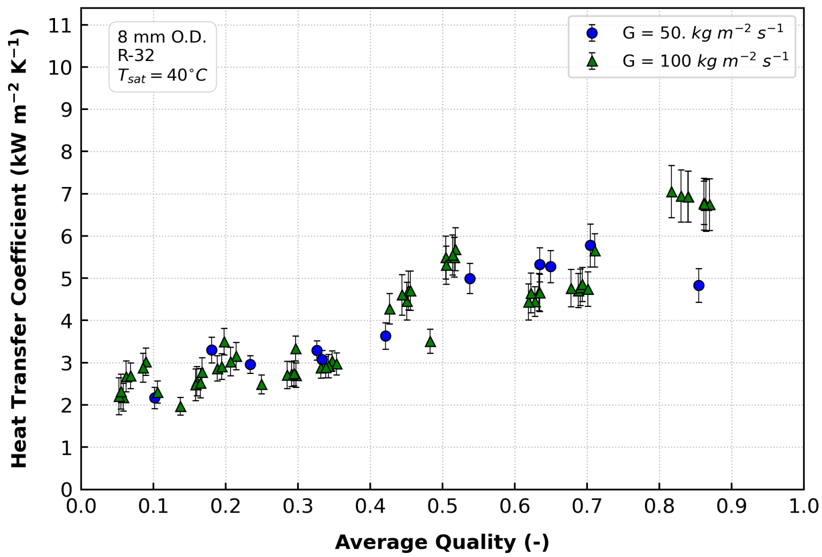

Figure 4.16: Heat transfer coefficients versus thermodynamic quality for R-32 condensing at $T_{sat} = 40\,°\mathrm{C}$.

more drastic for the 4 mm microfin tube. A more extensive data set with mass fluxes up to $300\,\mathrm{kg\,m^{-2}\,s^{-1}}$ or higher is needed for the 8 mm microfin tube, but this was not feasible with the current experimental facility.

For the 8 mm O.D. microfin tube, the Cavallini, Del Col, Mancin, et al. (2009) heat transfer correlation performs the best once again. The R-32 heat transfer coefficients are predicted with a MAPE of 16%. The correlations by Kedzierski and Goncalves (1999) and Yu and Koyama (1998) produced a MAPE of 41% and 26%, respectively. For R-454C, the Cavallini, Del Col, Mancin, et al. (2009) correlation without the SBG correction produces a MAPE of 49%, and the agreement improves to a MAPE of 16% after the SBG correction is applied as shown in Figures 4.21 and 4.22. In contrast with the 4 mm O.D. microfin tube, the larger 8 mm O.D. microfin

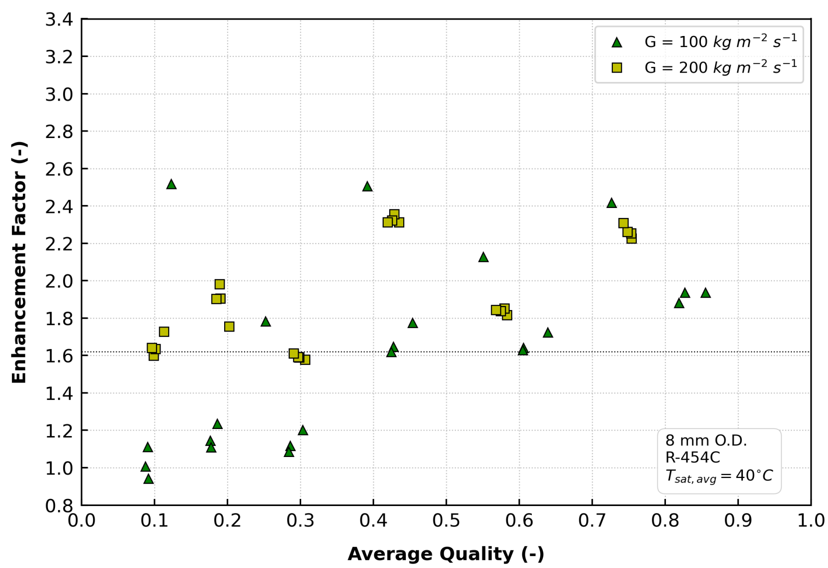

Figure 4.17: Enhancement factors for R-454C condensing at $T_{sat,avg} = 40\,^{\circ}$C.

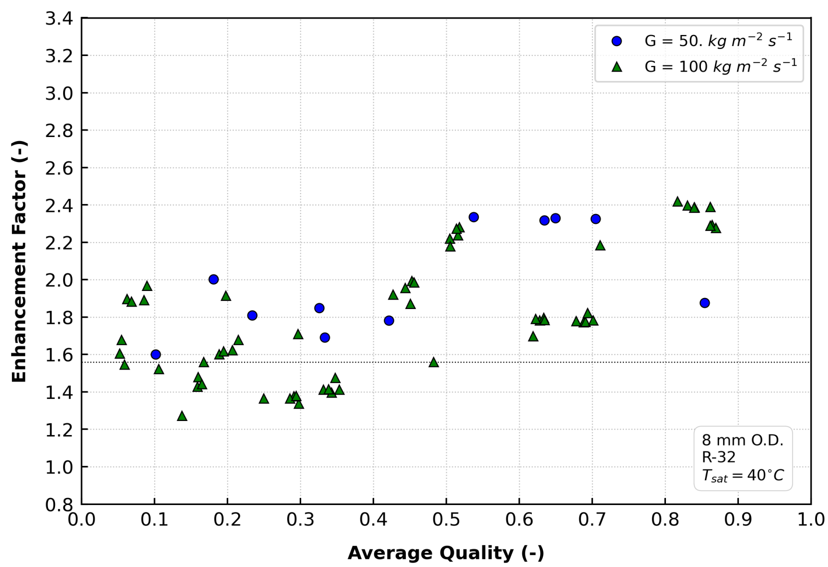

Figure 4.18: Enhancement factors for R-32 condensing at $T_{sat} = 40\,^{\circ}$C.

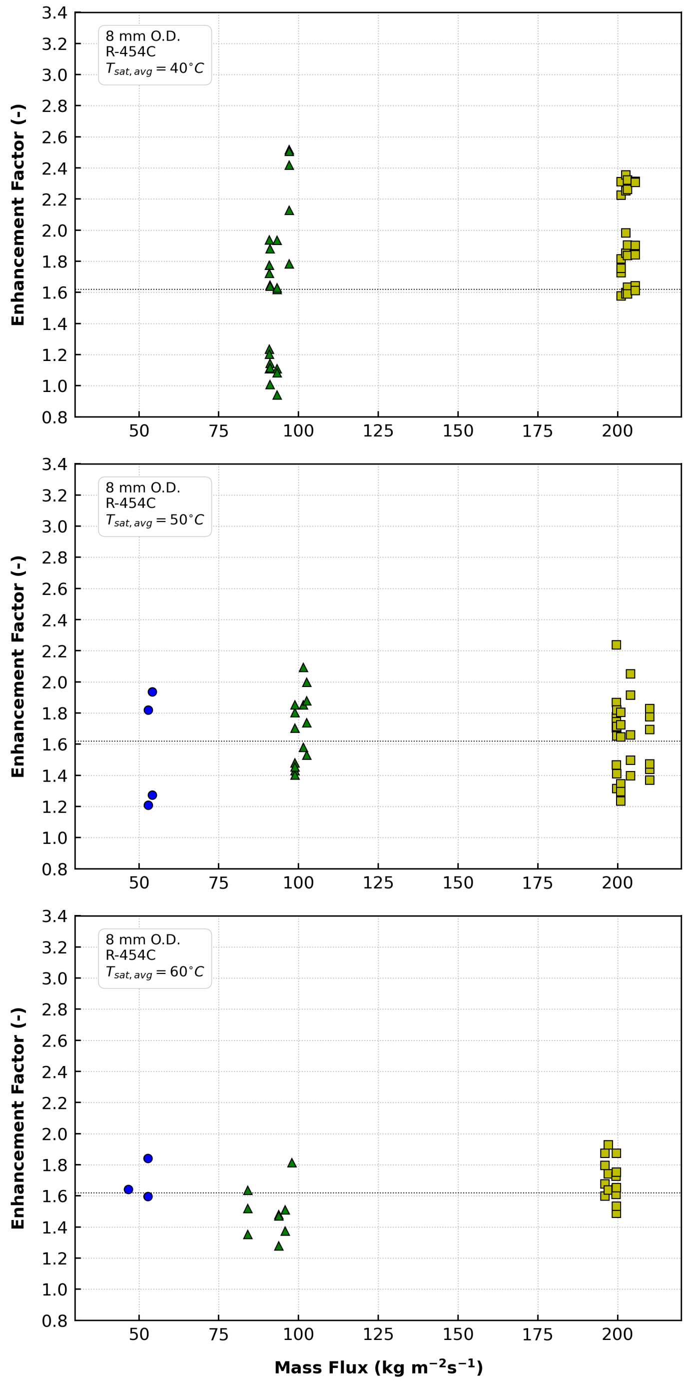

Figure 4.19: Enhancement factors versus mass flux for R-454C at $T_{sat} = 40, 50 and 60\,^{\circ}\mathrm{C}$.

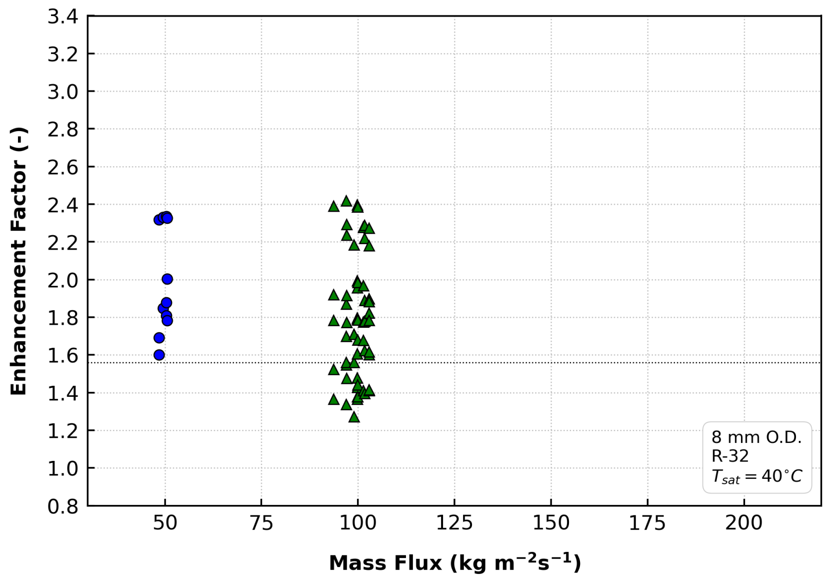

Figure 4.20: Enhancement factors plotted against mass flux for R-32 condensing at $T_{sat} = 40\,^{\circ}\mathrm{C}$.

tube does not mitigate the degradation in heat transfer performance associated with the mixture and it is recommended to use the SBG correction. As shown in Figures 4.4 and 4.5, the flow regimes in the 4 mm and 8 mm microfin tube are expected to be mostly annular and mostly stratified, respectively. For annular flow in the 4 mm microfin tube, the fins may protrude through the condensate film into the vapor bulk and the mass transfer resistance is mitigated. The secondary flow structures produced by the helical fin geometry also causes mixing between the vapor bulk and condensate which also serves to reduce the mass transfer resistance. Furthermore, the vapor quality at which the fins become flooded with condensate is lower in the 4 mm microfin tube as shown in Figure 4.6.

For condensation of R-454C in a smooth tube with a diameter of 4.7 mm, Jacob

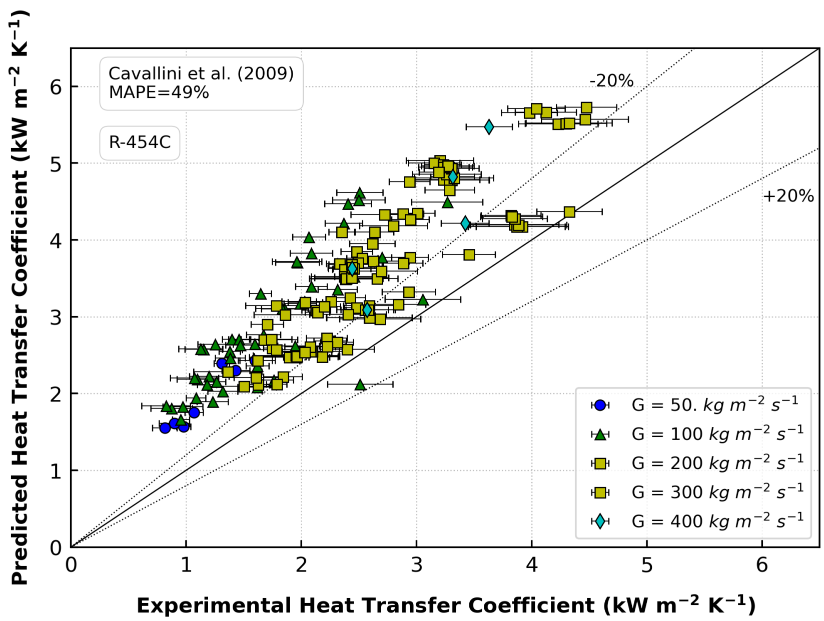

Figure 4.21: A comparison of measured heat transfer coefficients for R-454C against the Cavallini, Del Col, Mancin, et al. (2009) heat transfer correlation.

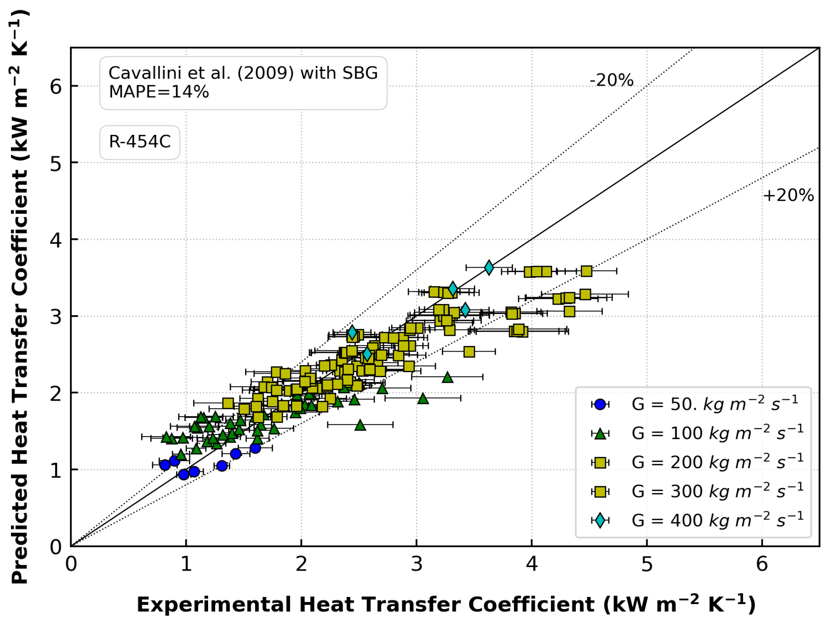

Figure 4.22: A comparison of measured heat transfer coefficients for R-454C against the Cavallini, Del Col, Mancin, et al. (2009) heat transfer correlation with the Bell and Ghaly (1974) correction applied.

and Fronk (2020) showed that the SBG correction improved the agreement between experimental heat transfer coefficients for R-454C and the Cavallini, Col, Doretti, et al. (2006) correlation. In their work, applying the SBG correction produced a 12% reduction, on average, in the heat transfer coefficients predicted by the Cavallini, Col, Doretti, et al. (2006) correlation. Since the SBG correction is not needed in the 4 mm microfin tube, the presence of the microfins on the inner surface of the tube must be counteracting the additional mass transfer resistance at the liquid-vapor interface.

4.4 Two-phase Frictional Pressure Drop

4.4.1 4 mm O.D. Microfin Tube

The frictional pressure drop for complete condensation was evaluated using the procedure outlined in Section 3.2.2. Experiments with a total pressure drop of less than 0.75 kPa are not reported in this study due to the limited accuracy and sensitivity of the differential pressure transducer at low differential pressures. Therefore, the penalty factors at mass fluxes of $100\,\mathrm{kg\,m^{-2}\,s^{-1}}$ are not shown. The frictional pressure gradients for condensing flows in the 8 mm O.D. microfin tube were near the 0.75 kPa threshold, therefore they are also not discussed here. Penalty factors are used to compare the frictional pressure drop in the microfin tube to a smooth tube. The smooth tube pressure drop is calculated using the Müller-Steinhagen and Heck (1986) correlation. Their correlation is applicable for two-phase flows in pipes and was checked against an extensive database of over 9300 data points. The penalty factors tend to increase with mass flux as shown in Figure 4.23. The penalty factors increase as the mass flux increases from 200 to $400\,\mathrm{kg\,m^{-2}\,s^{-1}}$, and then they remain relatively constant as the mass flux increases to $600\,\mathrm{kg\,m^{-2}\,s^{-1}}$. The frictional pressure drop in the microfin tube is greater than the smooth tube due to additional surface area on the inside of the tube. The fins also generate turbulence in the flow which leads to larger pressure drops. Additionally, the height of the fins, although they are relatively small, extend into the vapor bulk where the flow velocity is high which results in high shear at the fin tip. The penalty factors remain relatively constant for the higher mass fluxes from 400 to $600\,\mathrm{kg\,m^{-2}\,s^{-1}}$. At these high mass fluxes, the flow is already very turbulent so the contribution of the microfins to the overall flow turbulence is relatively low. For this reason, the penalty factors all remain around 2.6 with further increases in mass flux. The enhancement factor tends to increase as the mass flux is reduced, and the penalty factor tends to increase as the mass flux increases which suggests that the optimum operating condition for the 4 mm O.D. microfin tube occurs at a mass flux around $200\,\mathrm{kg\,m^{-2}\,s^{-1}}$.

The measured condensation frictional pressure drops were compared to correlations developed by Cavallini, Del Col, Longo, et al. (1997), Kedzierski and Goncalves (1999) and Han and Lee (2005). These correlations were developed specifically for condensation of refrigerants in horizontal microfin tubes. The Cavallini, Del Col, Longo, et al. (1997) correlation performs the best for all fluids in the 4 mm O.D. microfin tube with a MAPE of 24%, as shown in Figure 4.24. The correlation by

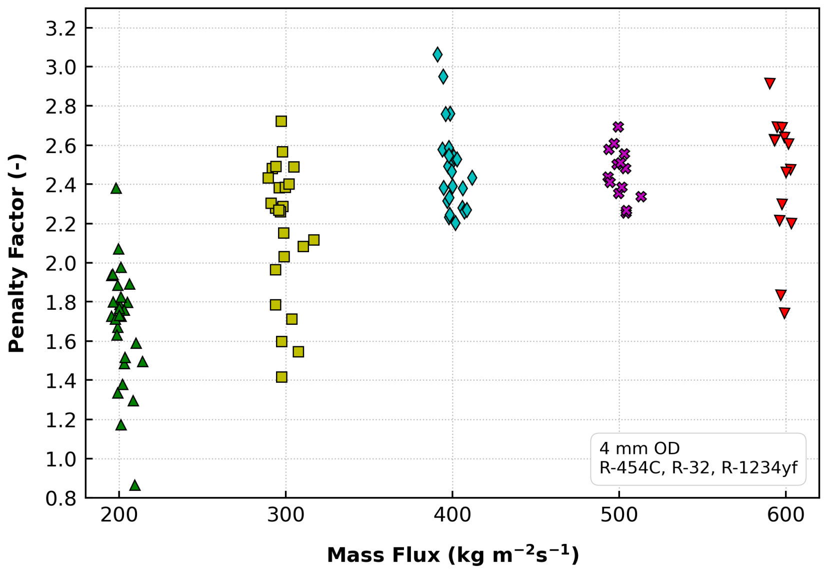

Figure 4.23: Penalty factors for R-454C, R-32, and R-1234yf in the 4 mm O.D. microfin tube plotted against mass flux.

Han and Lee (2005) predicted the experimental data with a MAPE of 32%, and the Kedzierski and Goncalves (1999) correlation predicted the data with a 59% MAPE.

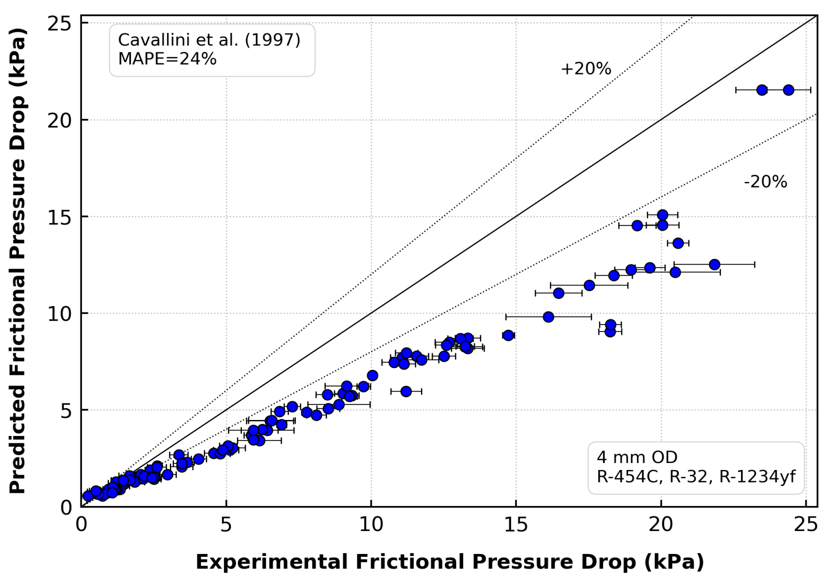

Figure 4.24: A comparison of the experimental frictional pressure gradients in the 4 mm O.D. microfin tube compared to the predictions by the Cavallini, Del Col, Doretti, et al. (1999) correlation.

Chapter 5: Conclusion

5.1 Summary of the research scope

International mandates and regulations have established a phase-out timeline for many refrigerants due to their harmful impacts on the environment. Near-azeotropic and zeotropic refrigerants have emerged in the HVAC&R industry as potential replacements for conventional HFC refrigerants because their composition can be adjusted to meet environmental regulations while still maintaining desirable thermophysical properties. There are many studies in the literature that investigate the heat transfer and pressure drop performance of these mixtures, but there are relatively few studies on condensation inside enhanced tubes that compare the performance of the refrigerant mixture to its individual components. Understanding the heat transfer and pressure drop performance characteristics of a working fluid is critical for accurately designing condensers with next-generation refrigerants. Through a survey of the literature, it was apparent that there is a lack of research on the condensation heat transfer and pressure drop performance in smaller diameter microfin tubes with next-generation refrigerant mixtures as the working fluid. Therefore, the overarching goal of this work is to fill this gap by studying condensation of the zeotropic refrigerant mixture R-454C in a 4 mm and 8 mm O.D. microfin tubes. The experimental data that results from this study will be made public for other researchers to use. Additionally, the experimental data is used to evaluate the predictive capabilities of condensation heat transfer and frictional pressure drop correlations from the literature. This evaluation will guide engineers in selecting the appropriate design correlations when working with R-454C, R-1234yf or R-32.

5.2 Conclusions

Heat transfer and pressure drop measurements were taken during in-tube condensation of R-454C, R-32 and R-1234yf in a horizontal 4 mm and 8 mm O.D. microfin tubes. The temperature glide of the zeotropic mixture R-454C is 7K at typical condenser operating pressures. Measurements were taken from a counter-flow tube-in-tube heat exchanger with cooling water flowing in the annulus and refrigerant flowing in the inner microfin tube. The test sections were divided into seven segments to measure quasi-local heat transfer coefficients along the length of the test section. The refrigerant enters the test section as a superheated vapor, then completely condenses in the test section and exits as a subcooled liquid.

The results of this study show that an optimum operating condition exists at lower mass fluxes, around $200\,\mathrm{kg\,m^{-2}\,s^{-1}}$, where the heat transfer enhancement due to the microfins is highest and the pressure drop penalty is lowest. A heat transfer correlation developed by Cavallini, Del Col, Mancin, et al. (2009) was found to predict experimental data with good agreement, and this correlation is recommended for condenser design applications. In the 4 mm microfin tube, the Bell and Ghaly (1974) (or SBG) correction is not needed to account for the additional mass transfer resistances associated with the refrigerant mixture R-454C. However, this correction is needed for the larger 8 mm microfin tube. The heat transfer enhancement mechanisms were found to counteract the additional mass transfer and sensible resistances in the smaller diameter tube, but not in the larger diameter tube. This demonstrates that low global warming potential refrigerant mixture R-454C is a viable candidate to replace other refrigerants specifically in the residential and commercial refrigeration and air conditioning applications. For the pure fluids, microfin tubes can be used to realize appreciable heat transfer enhancement to reduce the physical size of a condenser, increase the system thermodynamic efficiency by means of increased heat duty for constant compressor power, or maintain the same heat duty with a decrease in compressor power.

5.2.1 Contributions

This work will facilitate the implementation of commercially available microfin tubes in various HVAC&R systems and aid in the adoption of low global warming potential refrigerants and refrigerant mixtures. The experimental data produced during this study will be made available to the public to expand this work.

5.2.2 Recommendations for future work

This work is among a few studies that investigated condensation of a zeotropic mixture and its individual components in a helical microfin tube. This area of research can be advanced further in the following ways.

- Most of the condensation heat transfer and pressure drop experimental investigations in the literature are conducted in tubes around 9.52 mm in diameter. Further investigation with microfin tubes with smaller diameters would benefit this field of work.
- Only one zeotropic refrigerant mixture was studied in this investigation. There are many others on the market with larger and smaller temperature glides. The heat transfer performance in microfin tubes can be evaluated for varying temperature glides.
- A longer test section can be used for 8 mm microfin tube in this study. This would allow for complete condensation experiments at mass fluxes higher than $200\,\mathrm{kg\,m^{-2}\,s^{-1}}$.
- The refrigerants tested in this study were never mixed with lubricating oils. Oils are required for lubricating compressors and also influence heat transfer and pressure drop characteristics. Few studies have investigated this in microfin tubes.

Bibliography

Adelaja, Adekunle O. et al. (Dec. 2019). "Heat transfer, void fraction and pressure drop during condensation inside inclined smooth and microfin tubes". In: *Experimental Thermal and Fluid Science* 109, p. 109905. ISSN: 08941777. DOI: 10.1016/j.expthermflusci.2019.109905. URL: https://linkinghub.elsevier.com/retrieve/pii/S0894177719309665 (visited on 09/17/2020).

Amendment to the Montreal Protocol on Substances That Deplete the Ozone Layer (Oct. 15, 2016). URL: https://treaties.un.org/doc/Treaties/2016/10/20161015%2003-23%20PM/Ch_XXVII-2.f.pdf.

Azzolin, Marco et al. (July 2019). "Condensation of ternary low GWP zeotropic mixtures inside channels". In: *International Journal of Refrigeration* 103, pp. 77–90. ISSN: 01407007. DOI: 10.1016/j.ijrefrig.2019.03.021. URL: https://linkinghub.elsevier.com/retrieve/pii/S0140700719301203 (visited on 03/28/2020).

Bashar, M. Khairul et al. (Dec. 2020). "Condensation heat transfer of R1234yf in a small diameter smooth and microfin tube and development of correlation". In: *International Journal of Refrigeration* 120, pp. 331–339. ISSN: 01407007. DOI: 10.1016/j.ijrefrig.2020.09.002. URL: https://linkinghub.elsevier.com/retrieve/pii/S0140700720303741 (visited on 11/09/2020).

Bell, Kenneth J. and Mohamed A. Ghaly (1974). “An Approximate Generalized Design Method For Multicomponent/Partial Condensers”. In: *AIChE Symposium Series* 69.131, pp. 267–272.

Bhatia, Ranjeet S and Ralph L Webb (2001). “Numerical Study of Turbulent Flow and Heat Transfer in Micro-Fin Tubes - Part 1, Model Validation”. In: *Journal of Enhanced Heat Transfer* 8.5, pp. 291–304.

Bukasa, Jean-Pierre M. et al. (June 1, 2004). “Heat Transfer Performance During Condensation Inside Spiralled Micro-Fin Tubes”. In: *Journal of Heat Transfer* 126.3, pp. 321–328. ISSN: 0022-1481, 1528-8943. DOI: 10.1115/1.1737777. URL: https://asmedigitalcollection.asme.org/heattransfer/article/126/3/321/458172/Heat-Transfer-Performance-During-Condensation (visited on 06/08/2020).

Cavallini, A, G Censi, D Del Col, et al. (2002). “Heat Transfer Coefficients Of HFC Refrigerants During Condensation At High Temperature Inside An Enhanced Tube”. In: International Refrigeration and Air Conditioning Conference. Purdue University, p. 10. URL: http://docs.lib.purdue.edu/iracc/563.

Cavallini, A, L. Del Col D., G. A. Longo, et al. (1997). “Pressure drop during condensation and vaporisation of refrigerants inside enhanced tubes”. In: 15.1, pp. 3–10. (Visited on 11/25/2019).

Cavallini, A., G. Censi, D. Del Col, et al. (Jan. 2001). “Experimental investigation on condensation heat transfer and pressure drop of new HFC refrigerants (R134a, R125, R32, R410A, R236ea) in a horizontal smooth tube”. In: *International Journal of Refrigeration* 24.1, pp. 73–87. ISSN: 01407007. DOI: 10.1016/S0140-

7007(00)00070-0. URL: https://linkinghub.elsevier.com/retrieve/pii/S0140700700000700 (visited on 09/26/2019).

Cavallini, A., D. Del Col, L Doretti, et al. (1999). "A New Computational Procedure for Heat Transfer and Pressure Drop During Refrigerant Condensation Inside Enhanced Tubes". In: *Enhanced Heat Transfer* 6, pp. 441–456.

Cavallini, A., D. Del Col, S. Mancin, et al. (Jan. 2009). "Condensation of pure and near-azeotropic refrigerants in microfin tubes: A new computational procedure". In: *International Journal of Refrigeration* 32.1, pp. 162–174. ISSN: 01407007. DOI: 10.1016/j.ijrefrig.2008.08.004. URL: https://linkinghub.elsevier.com/retrieve/pii/S0140700708001539 (visited on 10/13/2019).

Cavallini, Alberto, Davide Del Col, Luca Doretti, et al. (Sept. 2006). "Condensation in Horizontal Smooth Tubes: A New Heat Transfer Model for Heat Exchanger Design". In: *Heat Transfer Engineering* 27.8, pp. 31–38. ISSN: 0145-7632, 1521-0537. DOI: 10.1080/01457630600793970. URL: https://www.tandfonline.com/doi/full/10.1080/01457630600793970 (visited on 09/27/2019).

Cavallini, Alberto, Davide Del Col, Simone Mancin, et al. (2006). "Thermal Performance of R410A Condensing in a Microfin Tube". In: International Refrigeration and Air Conditioning Conference. Purdue University, p. 10. URL: http://docs.lib.purdue.edu/iracc/806.

Chamra, L.M. et al. (June 1996). "Advanced micro-fin tubes for condensation". In: *International Journal of Heat and Mass Transfer* 39.9, pp. 1839–1846. ISSN: 00179310. DOI: 10.1016/0017-9310(95)00275-8. URL: https://linkinghub.elsevier.com/retrieve/pii/0017931095002758 (visited on 03/28/2020).

Colburn, A.P. and T.B. Drew (1937). "The condensation of mixed vapors". In: 33, pp. 197–215.

Colombo, L.P.M. et al. (Dec. 2012). "Flow patterns, heat transfer and pressure drop for evaporation and condensation of R134A in microfin tubes". In: *International Journal of Refrigeration* 35.8, pp. 2150–2165. ISSN: 01407007. DOI: 10.1016/j.ijrefrig.2012.08.019. URL: https://linkinghub.elsevier.com/retrieve/pii/S014070071200206X (visited on 05/18/2020).

Diani, Andrea, Pierfrancesco Brunello, et al. (May 2020). "R513A condensation heat transfer inside tubes: Microfin tube vs. smooth tube". In: *International Journal of Heat and Mass Transfer* 152, p. 119472. ISSN: 00179310. DOI: 10.1016/j.ijheatmasstransfer.2020.119472. URL: https://linkinghub.elsevier.com/retrieve/pii/S0017931019361472 (visited on 02/23/2020).

Diani, Andrea, Manuela Campanale, Alberto Cavallini, et al. (Feb. 2018). "Low GWP refrigerants condensation inside a 2.4 mm ID microfin tube". In: *International Journal of Refrigeration* 86, pp. 312–321. ISSN: 01407007. DOI: 10.1016/j.ijrefrig.2017.11.011. URL: https://linkinghub.elsevier.com/retrieve/pii/S0140700717304541 (visited on 03/28/2020).

Diani, Andrea, Manuela Campanale, and Luisa Rossetto (Nov. 2018). "Experimental study on heat transfer condensation of R1234ze(E) and R134a inside a 4.0 mm OD horizontal microfin tube". In: *International Journal of Heat and Mass Transfer* 126, pp. 1316–1325. ISSN: 00179310. DOI: 10.1016/j.ijheatmasstransfer.2018.06.047. URL: https://linkinghub.elsevier.com/retrieve/pii/S0017931018316740 (visited on 10/06/2019).

Diani, Andrea, Alberto Cavallini, et al. (Mar. 2017). "R1234yf condensation inside a 3.4 mm ID horizontal microfin tube". In: *International Journal of Refrigeration* 75, pp. 178–189. ISSN: 01407007. DOI: 10.1016/j.ijrefrig.2016.12.014. URL: https://linkinghub.elsevier.com/retrieve/pii/S0140700716304273 (visited on 09/26/2019).

Doretti, L. et al. (Mar. 2013). "Condensation flow patterns inside plain and microfin tubes: A review". In: *International Journal of Refrigeration* 36.2, pp. 567–587. ISSN: 01407007. DOI: 10.1016/j.ijrefrig.2012.10.021. URL: https://linkinghub.elsevier.com/retrieve/pii/S0140700712002812 (visited on 12/13/2019).

Eckels, S. J. and B. A. Tesene (1999a). "A Comparison of R-22, R-134a, R-410a, and R-407c Condensation Performance in Smooth and Enhanced Tubes: Part I, Heat Transfer". In: *ASHRAE Transactions: Research* 105.2, pp. 428–441. (Visited on 02/04/2020).

Eckels, Steven J. and Brian Tesene (2002). "Forced convective condensation of refrigerants R-502 and R-507 in smooth and enhanced tubes". In: *ASHRAE Transactions*. Vol. 108, pp. 627–638.

Eckels, Steven J. and Brian A. Tesene (1999b). "A comparison of R-22, R-134a, R-410a, and R-407c condensation performance in smooth and enhanced tubes: Part II, pressure drop". In: *ASHRAE Transactions*. Vol. 105, pp. 442–452.

Fronk, Brian M. and Srinivas Garimella (Mar. 2013). "In-tube condensation of zeotropic fluid mixtures: A review". In: *International Journal of Refrigeration* 36.2, pp. 534–561. ISSN: 01407007. DOI: 10.1016/j.ijrefrig.2012.11.030.

URL: https://linkinghub.elsevier.com/retrieve/pii/S0140700712003441 (visited on 11/24/2019).

Fronk, Brian M. and Srinivas Garimella (Oct. 2016). "Condensation of ammonia and high-temperature-glide ammonia/water zeotropic mixtures in minichannels – Part I: Measurements". In: *International Journal of Heat and Mass Transfer* 101, pp. 1343–1356. ISSN: 00179310. DOI: 10.1016/j.ijheatmasstransfer.2016.05.049. URL: https://linkinghub.elsevier.com/retrieve/pii/S0017931015317701 (visited on 03/28/2020).

Goto, M et al. (July 2001). "Condensation and evaporation heat transfer of R410A inside internally grooved horizontal tubes". In: *International Journal of Refrigeration* 24.7, pp. 628–638. ISSN: 01407007. DOI: 10.1016/S0140-7007(00)00087-6. URL: https://linkinghub.elsevier.com/retrieve/pii/S0140700700000876 (visited on 10/21/2019).

Graham, D. et al. (June 1999). "Heat transfer and pressure drop during condensation of refrigerant 134a in an axially grooved tube". In: *International Journal of Heat and Mass Transfer* 42.11, pp. 1935–1944. ISSN: 00179310. DOI: 10.1016/S0017-9310(98)00307-X. URL: https://linkinghub.elsevier.com/retrieve/pii/S001793109800307X (visited on 09/27/2019).

Han, D. and Kyu-Jung Lee (Aug. 2005). "Experimental study on condensation heat transfer enhancement and pressure drop penalty factors in four microfin tubes". In: *International Journal of Heat and Mass Transfer* 48.18, pp. 3804–3816. ISSN: 00179310. DOI: 10.1016/j.ijheatmasstransfer.2005.02.041. URL:

https://linkinghub.elsevier.com/retrieve/pii/S0017931005003017 (visited on 02/03/2020).

Hirose, Masataka et al. (June 2018). "Development of the general correlation for condensation heat transfer and pressure drop inside horizontal 4 mm small-diameter smooth and microfin tubes". In: *International Journal of Refrigeration* 90, pp. 238–248. ISSN: 01407007. DOI: 10.1016/j.ijrefrig.2018.04.014. URL: https://linkinghub.elsevier.com/retrieve/pii/S0140700718301208 (visited on 03/28/2020).

Infante Ferreira, C.A. et al. (June 2003). "R404A condensing under forced flow conditions inside smooth, microfin and cross-hatched horizontal tubes". In: *International Journal of Refrigeration* 26.4, pp. 433–441. ISSN: 01407007. DOI: 10.1016/S0140-7007(02)00156-1. URL: https://linkinghub.elsevier.com/retrieve/pii/S0140700702001561 (visited on 01/09/2020).

Ishikawa, Seiichi et al. (2002). "Heat Transfer and Pressure Drop During Evaporation and Condensation of HCFC22 in Horizontal Copper Tubes with Many Inner Fins". In: *Journal of Enhanced Heat Transfer* 9.1, pp. 17–23. (Visited on 12/18/2019).

Jacob, Tabeel A. (Sept. 1, 2020). "Investigation of In-tube Non-equilibrium Condensation of Low Global Warming Potential Refrigerants". PhD thesis. Oregon State University. 203 pp.

Jacob, Tabeel A. and Brian M. Fronk (Oct. 20, 2020). "In-Tube condensation of zeotropic refrigerant R454C from superheated vapor to subcooled liquid". In: *Science and Technology for the Built Environment* 26.9, pp. 1177–1190. ISSN:

2374-4731, 2374-474X. DOI: 10.1080/23744731.2020.1804281. URL: https://www.tandfonline.com/doi/full/10.1080/23744731.2020.1804281 (visited on 09/20/2020).

Jacob, Tabeel A., Ethan P. Matty, et al. (July 2019). "Experimental investigation of in-tube condensation of low GWP refrigerant R450A using a fiber optic distributed temperature sensor". In: *International Journal of Refrigeration* 103, pp. 274–286. ISSN: 01407007. DOI: 10.1016/j.ijrefrig.2019.04.021. URL: https://linkinghub.elsevier.com/retrieve/pii/S014070071930177X (visited on 02/20/2020).

— (Aug. 2020). "Comparison of R404A condensation heat transfer and pressure drop with low global warming potential replacement candidates R448A and R452A". In: *International Journal of Refrigeration* 116, pp. 9–22. ISSN: 01407007. DOI: 10.1016/j.ijrefrig.2020.03.014. URL: https://linkinghub.elsevier.com/retrieve/pii/S0140700720301298 (visited on 07/20/2020).

Jasiński, Piotr (2011). "Numerical optimization of flow-heat ducts with helical micro-fins, using Entropy Generation Minimization (EGM) method." In: 9th IASME/WSEAS International Conference on Fluid Mechanics and Aerodynamics, pp. 47–54.

Jung, Dongsoo et al. (Jan. 2004). "Flow condensation heat transfer coefficients of R22, R134a, R407C, and R410A inside plain and microfin tubes". In: *International Journal of Refrigeration* 27.1, pp. 25–32. ISSN: 01407007. DOI: 10.1016/S0140-7007(03)00122-1. URL: https://linkinghub.elsevier.com/retrieve/pii/S0140700703001221 (visited on 03/23/2020).

Kedzierski, M. A. and J. M. Goncalves (1999). "Horizontal Convective Condensation of Alternative Refrigerants Within a Micro-Fin Tube". In: *Enhanced Heat Transfer* 6, pp. 161–178. (Visited on 10/06/2019).

Khanpara, J. C. et al. (1986). "Augmentation of R-113 in-tube condensation with micro-fin tubes". In: Heat Transfer in Air Conditioning and Refrigeration Equipment. Portland, OR. URL: https://access.library.oregonstate.edu/pdf/1180267.pdf.

Kim, Man-Hoe and Joeng-Seob Shin (Sept. 2005). "Condensation heat transfer of R22 and R410A in horizontal smooth and microfin tubes". In: *International Journal of Refrigeration* 28.6, pp. 949–957. ISSN: 01407007. DOI: 10.1016/j.ijrefrig.2005.01.017. URL: https://linkinghub.elsevier.com/retrieve/pii/S0140700705000502 (visited on 03/23/2020).

Klein, Sanford and Gregory Nellis (2020). *Engineering Equation Solver*.

Kline, S. J. and F. A. McClintock (Jan. 1953). "Describing uncertainties in single-sample experiments". In: *Mechanical Engineering*, pp. 3–8.

Kondou, Chieko (Nov. 26, 2019). "Heat transfer and pressure drop of R1123/R32 (40/60 mass%) flow in horizontal microfin tubes during condensation and evaporation". In: *Science and Technology for the Built Environment* 25.10, pp. 1281–1291. ISSN: 2374-4731, 2374-474X. DOI: 10.1080/23744731.2019.1642096. URL: https://www.tandfonline.com/doi/full/10.1080/23744731.2019.1642096 (visited on 09/19/2020).

Kondou, Chieko et al. (July 4, 2015). "Condensation and evaporation of R32/R1234ze(E) and R744/R32/R1234ze(E) flow in horizontal microfin tubes". In: *Science* *and Technology for the Built Environment* 21.5, pp. 564–577. ISSN: 2374-4731, 2374-474X. DOI: 10.1080/23744731.2015.1023163. URL: http://www.tandfonline.com/doi/full/10.1080/23744731.2015.1023163 (visited on 10/06/2019).

Koyama, Shigeru et al. (1990). "Condensation heat transfer of binary refrigerant mixtures of R22 and Rl14 inside a horizontal tube with internal spiral grooves". In: *International Journal of Refrigeration* 13, p. 8.

Lambrechts, Adriaan et al. (July 1, 2006). "Heat Transfer Performance During Condensation Inside Horizontal Smooth, Micro-Fin and Herringbone Tubes". In: *Journal of Heat Transfer* 128.7, pp. 691–700. ISSN: 0022-1481, 1528-8943. DOI: 10.1115/1.2194038. URL: https://asmedigitalcollection.asme.org/heattransfer/article/128/7/691/467498/Heat-Transfer-Performance-During-Condensation (visited on 01/06/2020).

Lemmon, Eric W. et al. (2018). *NIST Standard Reference Database 23: Reference Fluid Thermodynamic and Transport Properties-REFPROP*. Version 10.0. URL: https://www.nist.gov/srd/refprop.

Li, Guan-Qiu, Zan Wu, et al. (Feb. 2012). "Experimental investigation of condensation in micro-fin tubes of different geometries". In: *Experimental Thermal and Fluid Science* 37, pp. 19–28. ISSN: 08941777. DOI: 10.1016/j.expthermflusci.2011.09.008. URL: https://linkinghub.elsevier.com/retrieve/pii/S0894177711001907 (visited on 09/30/2020).

Li, Puxuan, Matthew Campbell, et al. (June 2019). "Relationship between turbulent structures and heat transfer in microfin enhanced surfaces using large eddy simulations and particle image velocimetry". In: *International Journal of Heat and Mass Transfer* 136, pp. 1282–1298. ISSN: 00179310. DOI: 10.1016/j.ijheatmasstransfer.2019.03.063. URL: https://linkinghub.elsevier.com/retrieve/pii/S0017931018363257 (visited on 07/20/2020).

Liebenberg, Leon and Josua P. Meyer (Nov. 2006). "The characterization of flow regimes with power spectral density distributions of pressure fluctuations during condensation in smooth and micro-fin tubes". In: *Experimental Thermal and Fluid Science* 31.2, pp. 127–140. ISSN: 08941777. DOI: 10.1016/j.expthermflusci.2006.03.023. URL: https://linkinghub.elsevier.com/retrieve/pii/S089417770600046X (visited on 03/26/2020).

— (June 2008). "Refrigerant Condensation Flow Regimes in Enhanced Tubes and Their Effect on Heat Transfer Coefficients and Pressure Drops". In: *Heat Transfer Engineering* 29.6, pp. 506–520. ISSN: 0145-7632, 1521-0537. DOI: 10.1080/01457630801891532. URL: http://www.tandfonline.com/doi/abs/10.1080/01457630801891532 (visited on 01/06/2020).

Liu, Jiayao et al. (May 2020). "Diabatic visualization study of R245fa two phase flow pattern characteristics in horizontal smooth and microfin tube". In: *International Journal of Heat and Mass Transfer* 152, p. 119513. ISSN: 00179310. DOI: 10.1016/j.ijheatmasstransfer.2020.119513. URL: https://linkinghub.elsevier.com/retrieve/pii/S0017931019356108 (visited on 07/20/2020).

Mohseni, S.G. and M.A. Akhavan-Behabadi (Oct. 2011). "Visual study of flow patterns during condensation inside a microfin tube with different tube inclinations". In: *International Communications in Heat and Mass Transfer*

38.8, pp. 1156–1161. ISSN: 07351933. DOI: 10.1016/j.icheatmasstransfer.2011.04.032. URL: https://linkinghub.elsevier.com/retrieve/pii/S0735193311001102 (visited on 08/15/2020).

Müller-Steinhagen, H and K Heck (Nov. 1986). "A simple friction pressure drop correlation for two-phase flow in pipes". In: *Chemical Engineering and Processing: Process Intensification* 20.6, pp. 297–308. ISSN: 02552701. DOI: 10.1016/0255-2701(86)80008-3. URL: https://linkinghub.elsevier.com/retrieve/pii/0255270186800083 (visited on 02/17/2020).

Nozu, S. and H. Honda (Feb. 1, 2000). "Condensation of Refrigerants in Horizontal, Spirally Grooved Microfin Tubes: Numerical Analysis of Heat Transfer in the Annular Flow Regime". In: *Journal of Heat Transfer* 122.1, pp. 80–91. ISSN: 0022-1481, 1528-8943. DOI: 10.1115/1.521439. URL: https://asmedigitalcollection.asme.org/heattransfer/article/122/1/80/459127/Condensation-of-Refrigerants-in-Horizontal (visited on 01/09/2020).

Oh, Se-Yoon and Arthur E. Bergles (2002). "Visualization of the Effects of Spiral Angle on the Enhancement of In-Tube Flow Boiling in MicrofinTubes". In: *ASHRAE Transactions*. Vol. 108, pp. 509–515.

Olivier, Jonathan A. et al. (June 2007). "Heat transfer, pressure drop, and flow pattern recognition during condensation inside smooth, helical micro-fin, and herringbone tubes". In: *International Journal of Refrigeration* 30.4, pp. 609–623. ISSN: 01407007. DOI: 10.1016/j.ijrefrig.2006.11.003. URL: https://linkinghub.elsevier.com/retrieve/pii/S0140700706002301 (visited on 03/28/2020).

Opteon XL20 (2016). URL: https://www.opteon.com/en/-/media/files/opteon/opteon-xl20-pib-en.pdf.

Patil, P. A. (Mar. 12, 2012). "Performance Analysis of HFC-404A Vapor Compression Refrigeration System Using Shell and U-Tube Smooth and Micro-Fin Tube Condensers". In: *Experimental Heat Transfer* 25.2, pp. 77–91. ISSN: 0891-6152, 1521-0480. DOI: 10.1080/08916152.2011.562343. URL: http://www.tandfonline.com/doi/abs/10.1080/08916152.2011.562343 (visited on 11/16/2020).

Ravigururajan, T.S. and A.E. Bergles (July 1996). "Development and verification of general correlations for pressure drop and heat transfer in single-phase turbulent flow in enhanced tubes". In: *Experimental Thermal and Fluid Science* 13.1, pp. 55–70. ISSN: 08941777. DOI: 10.1016/0894-1777(96)00014-3. URL: https://linkinghub.elsevier.com/retrieve/pii/0894177796000143 (visited on 10/13/2019).

Regulation (EU) No 517/2014 of the European Parliament and of the Council of 16 April 2014 on fluorinated greenhouse gases and repealing Regulation (EC) No 842/2006 (May 20, 2014). URL: https://eur-lex.europa.eu/legal-content/EN/TXT/PDF/?uri=CELEX:32014R0517&from=EN.

Royal, J. H. and A. E. Bergles (Feb. 1978). "Augmentation of Horizontal In-Tube Condensation by Means of Twisted-Tape Inserts and Internally Finned Tubes". In: *Journal of Heat Transfer* 100.1, pp. 17–24. (Visited on 12/18/2019).

Shizuya, M. et al. (May 1995). “Condensation of Nonazeotropic Binary Refrigerant Mixtures Including R22 as a More Volatile Component Inside a Horizontal Tube”. In: *Journal of Heat Transfer* 117.2, pp. 538–543. (Visited on 01/09/2020).

Smit, F. J. et al. (Dec. 1, 2002). “Heat Transfer Coefficients During Condensation of the Zeotropic Refrigerant Mixture HCFC-22/HCFC-142b”. In: *Journal of Heat Transfer* 124.6, pp. 1137–1146. ISSN: 0022-1481, 1528-8943. DOI: `10.1115/1.1484108`. URL: `https://asmedigitalcollection.asme.org/heattransfer/article/124/6/1137/460020/Heat-Transfer-Coefficients-During-Condensation-of` (visited on 03/29/2020).

Tang, Liangyou et al. (2000). “Flow condensation in smooth and micro-fin tubes with HCFC-22, HFC-134a and HFC-410A refrigerants”. In: *Enhanced Heat Transfer* 7, pp. 289–310. URL: `https://access.library.oregonstate.edu/pdf/1163990.pdf`.

Webb, D.R., M. Fahrner, et al. (Oct. 1996). “The relationship between the colburn and silver methods of condenser design”. In: *International Journal of Heat and Mass Transfer* 39.15, pp. 3147–3156. ISSN: 00179310. DOI: `10.1016/0017-9310(96)00001-4`. URL: `https://linkinghub.elsevier.com/retrieve/pii/0017931096000014` (visited on 10/23/2019).

Webb, Ralph L. and Nae-Hyun Kim (2005). *Principles of Enhanced Heat Transfer*. 2nd ed. Taylor & Francis. 824 pp.

Wu, Zan and Bengt Sundén (Feb. 1, 2016). “Frictional Pressure Drop Correlations for Single-Phase Flow, Condensation, and Evaporation in Microfin Tubes”. In: *Journal of Heat Transfer* 138.2, p. 022901. ISSN: 0022-1481, 1528-8943. DOI:

10.1115/1.4031268. URL: https://asmedigitalcollection.asme.org/heattransfer/article/doi/10.1115/1.4031268/384403/Frictional-Pressure-Drop-Correlations-for (visited on 09/30/2020).

Wu, Zan, Bengt Sundén, et al. (May 1, 2014). “Convective Condensation Inside Horizontal Smooth and Microfin Tubes”. In: *Journal of Heat Transfer* 136.5, p. 051504. ISSN: 0022-1481, 1528-8943. DOI: 10.1115/1.4026370. URL: https://asmedigitalcollection.asme.org/heattransfer/article/doi/10.1115/1.4026370/373598/Convective-Condensation-Inside-Horizontal-Smooth (visited on 10/12/2019).

Yu, J and S Koyama (1998). “Condensation Heat Transfer of Pure Refrigerants in Microfin Tubes”. In: International Refrigeration and Air Conditioning Conference. Purdue University, p. 7.

Zivi, S.M. (1964). “Estimation of steady state steam void fraction by means of the principle of minimum entropy generation”. In: *Journal of Heat Transfer* 86, pp. 247–252.

APPENDICES